

Solution and Solid-State Studies of Alkali Metal Aggregate Assemblies

John Jacob Morris

Publication Date

07-04-2008

License

This work is made available under a All Rights Reserved license and should only be used in accordance with that license.

Citation for this work (American Psychological Association 7th edition)

Morris, J. J. (2008). *Solution and Solid-State Studies of Alkali Metal Aggregate Assemblies* (Version 1). University of Notre Dame. <https://doi.org/10.7274/br86b27956f>

This work was downloaded from CurateND, the University of Notre Dame's institutional repository.

For more information about this work, to report or an issue, or to preserve and share your original work, please contact the CurateND team for assistance at curate@nd.edu.

CHAPTER 5

SYSTEMATIC STUDY OF *ORTHO*-SUBSTITUTED ALKALI METAL ARYLOXIDES AGGREGATES HIGHLIGHTED BY THEIR USE IN HIGH- CONNECTIVITY NETWORKS AND ADVENTITIOUS WATER ENCAPSULATION

5.1 Introduction

During our targeted synthesis of high-connectivity networks using alkali metal aryloxide aggregates as outlined in the previous chapter, we studied the viability of using *ortho*-substituted aryloxides. We reasoned that the series of phenols shown in Figure 5.1 would be potentially good starting materials because the steric bulk from the substituent on only one side of the aryloxide ring would give a high degree of control over the localized aggregate while still allowing a large number of divergent Lewis bases to coordinate to each metal.

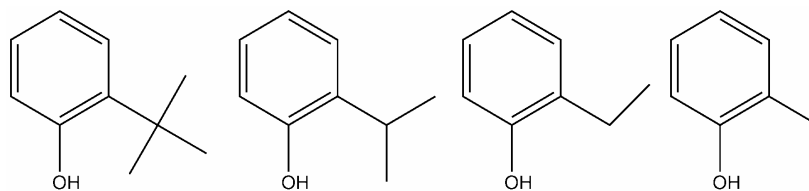


Figure 5.1 *Ortho*-substituted phenols used in this chapter.

The initial aim of the work outlined in this chapter was to explore the viability of using *ortho*-substituted aryloxide ligands in alkali metal aggregates for the construction of high-connectivity networks. As was discussed in the last chapter, one approach to

achieve the goal of high-connectivity networks is to create smaller aggregates with a large number of points for network extension.¹ This chapter will further explore the relationship between the localized aggregate and the resulting network connectivity.

An unexpected avenue of study also resulted during this research. Specifically, some of the complexes prepared were found to contain encapsulated water. In fact, these are the first structurally characterized examples of water being encapsulated within alkali metal cage aggregates. The second aim of this chapter, therefore, is to explore this unusual behavior for alkali metal aryloxide aggregates.

Alkali metal complexes are notoriously air- and moisture-sensitive.² Indeed, despite their best efforts a relatively frequent occurrence for researchers in *s*-block organometallic chemistry is the unanticipated appearance of O^{2-} , O_2^{2-} and OH^- anions as components of complex crystal structures.³ These species normally result from reaction of the highly oxophilic metal reagents with adventitious water or dioxygen. These observations are important as the formation of such mixed-anion complexes may significantly alter the reactivity and selectivity of the parent reagent.⁴ Also, the deliberate generation of these small anions has been used to stabilize large aggregates of main group complexes, where they act as points of cage ‘nucleation’.⁵ In comparison, there are no reports of neutral water encapsulation by an alkali metal cage aggregate.⁶ However, the formation of water-containing supramolecular capsules is well-known for self-assembled cages using transition metals and organic linkers.⁷ Since the neutral water molecule carries a pair of hydrogen centers it would be expected to create substantial repulsive interactions with surrounding highly electropositive alkali metal ions. Nevertheless, water is a ubiquitous ligand for alkali metal salts, with hundreds of known crystal structures.⁸

Most commonly, it acts as a terminal ligand, but it can also serve as a μ^2 - or even a μ^3 -bridge.

5.2 Reactions of 2-*tert*-Butylphenol

5.2.1 Synthesis

The equimolar reaction of 2-*tert*-butylphenol with potassium hexamethyldisilazide in 1,4-dioxane or THF resulted in the instant formation of a precipitate, which dissolved on vigorous heating. High-quality crystals of both solvates, $[\{(2\text{-}t\text{Bu-C}_6\text{H}_4\text{OK})_6\supset(\text{H}_2\text{O})\}\cdot(\text{dioxane})_4]_\infty$ (**5.1**) and $[\{(2\text{-}t\text{Bu-C}_6\text{H}_4\text{OK})_6\supset(\text{H}_2\text{O})\}\cdot(\text{THF})_6]$ (**5.2**), were grown from the reaction solution after optimizing their concentrations and temperatures for crystal growth. Subsequent equimolar reactions of 2-*tert*-butylphenol with $[\text{RbOBu}^t\cdot\text{Bu}^t\text{OH}]_\infty$ or NaH under similar crystallization conditions gave high-quality crystals of $[\{[(2\text{-}t\text{Bu-C}_6\text{H}_4\text{ORb})_6\supset(\text{H}_2\text{O})]\cdot(\text{dioxane})_4\}\cdot(\text{dioxane})]_\infty$ (**5.3**) and $[\{(2\text{-}t\text{Bu-C}_6\text{H}_4\text{ONa})_6\supset(\text{H}_2\text{O})\}\cdot(\text{dioxane})_3]_\infty$ (**5.4**). The following subsections describe the molecular and extended structures of all four complexes as well as the solution behavior of **5.1** and **5.2**.

5.2.2 Molecular Structure of Potassium 2-*tert*-Butylphenoxide Dioxane

Single-crystal X-ray diffraction analysis of **5.1** revealed the formation of a hexameric ‘drum’ aggregate, coordinated by six dioxane molecules. Two of the solvents terminally bind to the aggregate, while the remaining four dioxanes bridge to neighboring hexamers, leading to formation of a two-dimensional 4^4 -net.

Refinement of the X-ray data indicated a substantial residual peak near the center of the trimeric K_3O_3 ring of the asymmetric unit (Figure 5.2a). The most reasonable assignment for this site is the unexpected inclusion of a water molecule, as anion incorporation would render the complex charged. Symmetry expansion through the crystallographic inversion center leads to a pair of water molecules, each with a partial occupancy of ~50% (the oxygen centers are nominally separated by 1.28 Å). Thus, each hexamer in the crystalline lattice contains a single encapsulated water molecule, giving the molecular formula $[\{(2\text{-}^t\text{Bu-C}_6\text{H}_4\text{OK})_6\supset(\text{H}_2\text{O})\}\cdot(\text{diox})_4]_\infty$ (Figure 5.2b).

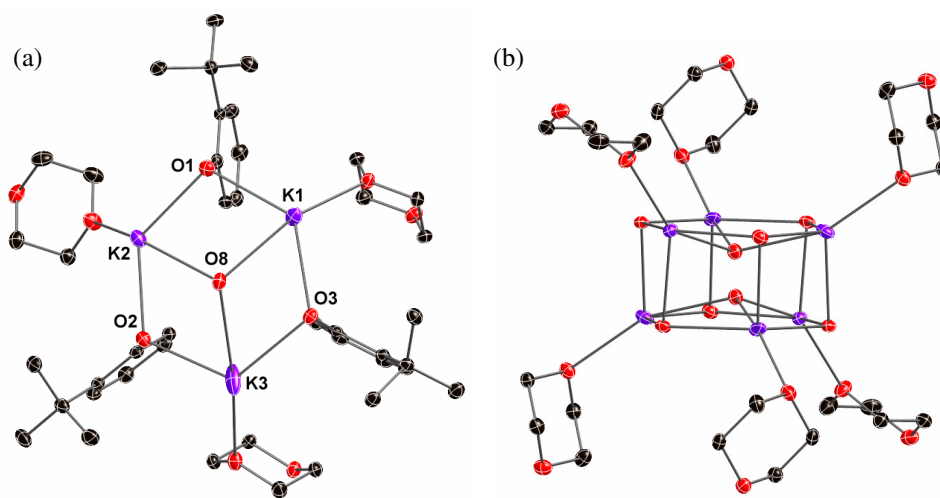


Figure 5.2 Structure of $[\{(2\text{-}^t\text{Bu-C}_6\text{H}_4\text{OK})_6\supset(\text{H}_2\text{O})\}\cdot(\text{dioxane})_4]$, **5.1**, showing (a) the asymmetric unit with hydrogen atoms removed for clarity, and (b) the prismatic hexamer highlighting the two disordered water sites within the aggregate and the six coordinated dioxanes. The carbon atoms of the aryloxide backbone are removed for clarity.

Considering the unique nature of the neutral molecular encapsulation within **5.1** we wished to unambiguously identify the guest present. This proved to be problematic by conventional means. The hydrogen positions could not be assigned from the X-ray data due to the location of the guest molecule over two sites. Also, ^1H NMR and IR analyses were unhelpful due to broadening of the signals (see subsections 5.2.3 and 5.3.3). The use

of neutron diffraction analysis was then targeted, as this technique is ideally suited for the location of hydrogen atoms. Subsequently, neutron diffraction data of **5.1** were obtained at the Intense Pulsed Neutron Source at Argonne National Laboratory using a time-of-flight Laue single-crystal diffractometer (neutron diffraction structure is labeled **5.1_n**).^{9,10} The atomic positions of the X-ray diffraction structure were used as a starting point in the refinement. Due to the large number of parameter variables, a joint refinement using X-ray and neutron reflections was used in the final model. However, only the neutron data was used to calculate the difference Fourier map in order to find all hydrogen atom positions. As illustrated in Figure 5.3, the refinement of **5.1_n** clearly identified the central guest molecule to be neutral water. In turn, an analysis of the metrical parameters within **5.1_n** provides valuable insights into the stabilization of this unusual structure.

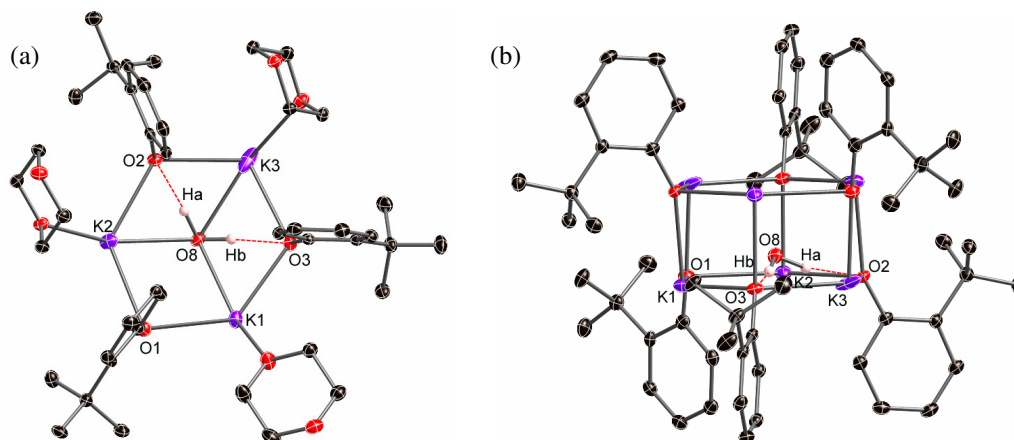


Figure 5.3 Structure of $[(2\text{-}t\text{Bu-C}_6\text{H}_4\text{OK})_6\supset(\text{H}_2\text{O})]\cdot(\text{dioxane})_4$, **5.1_n**, showing (a) the asymmetric unit with hydrogen atoms removed for clarity, and (b) the prismatic hexamer highlighting one water site within the aggregate with non-water hydrogens and dioxanes removed for clarity.

The two hydrogen atoms of the water molecule, Ha and Hb, have bond distances of 0.963(16) and 1.009(16) Å, to the central oxygen atom, O8, with an Ha-O8-Hb angle

of $108.0(13)^\circ$. Therefore, encapsulation by the hexameric prism does not significantly perturb the structure of the water molecule.¹¹ Each hydrogen of the water has a close interaction to a neighboring aryloxy oxygen, with distances of $1.726(16)$ Å for Ha-O2 and $1.721(17)$ Å for Hb-O3; and with angles of 167.69° for O8-Ha-O2 and 169.94° for O8-Hb-O3. These data support the formation of strong hydrogen bonds within the cage.¹¹

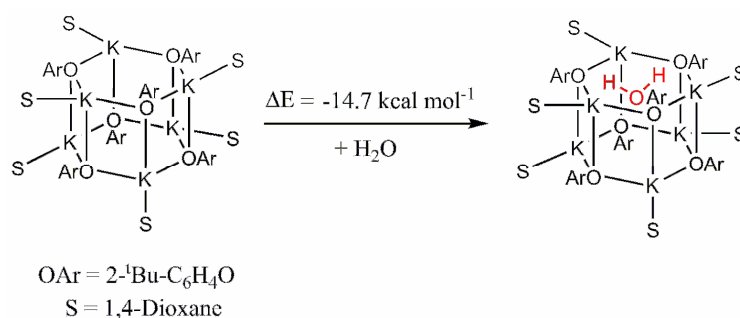
The two K_3O_3 rings of the hexameric prism define almost perfect planes, and the oxygen of the water molecule is asymmetrically located at distances of 1.88 and 0.68 Å between these mean planes. In turn, this leads to relatively short distances of $2.730(2)$, $2.751(2)$ and $2.723(2)$ Å between O8 of the water molecule and the three potassium centers of the closest ring K1, K2 and K3 respectively (the remaining K-O8 distances are all >3 Å). These internal K-O interactions are comparable with the mean K-O_{Ar} distance of 2.657 Å (range $2.521(1)$ - $2.761(1)$ Å) (Table 5.1).

TABLE 5.1KEY BOND LENGTHS [\AA] FOR **5.1-5.10**. MEAN DISTANCES ARE IN BRACKETS

	M-O_{Ar}	M-O_{Solvate}	M-O_{H2O}
5.1_n	2.521(1) - 2.761(1) <2.657>	2.606(2) - 2.619(2) <2.614>	2.723(2) - 2.751(2) <2.735>
5.2	2.562(2) - 2.841(2) <2.704>	2.646(2) - 2.736(3) <2.690>	2.833(4) - 2.973(4) <2.915>
5.3	2.781(2) - 3.036(3) <2.851>	2.850(3) - 2.960(7) <2.881>	2.91(3) - 2.96(2) <2.94>
5.4	2.277(1) - 2.440(1) <2.378>	2.278(1)	2.360(6)
5.5	2.568(3) - 2.792(3) <2.670>	2.679(3) - 3.018(4) <2.769>	2.779(11) - 2.876(11) <2.828>
5.6	2.559(1) - 2.944(1) <2.733>	2.594(3) - 2.883(1) <2.718>	—
5.7	2.520(1) - 2.908(1) <2.692>	2.644(1) - 2.971(1) <2.756>	2.727(1) - 2.883(1) <2.801>
5.8	2.690(2) - 3.161(2) <2.867>	2.791(2) - 3.315(2) <2.963>	—
5.9	2.565(2) - 2.927(5) <2.705>	2.63(2) - 2.846(9) <2.735>	—
5.10	2.594(6) - 2.757(5) <2.652>	2.651(6) - 2.841(6) <2.723>	—

Although there are two water sites within the aggregate, the neutron data of **5.1_n** indicates that the water molecule is not rotationally disordered. The neutron Fourier map shows only two clearly defined *holes* where the hydrogen could be located. Also, K3 and K3' have a noticeably elongated thermal ellipsoids compared to the other potassiums. These metal sites lie between the two hydrogen atoms of the water molecule. This suggests that the aggregate has some flexibility depending on the location of the water molecule. Since the water molecule equally occupies the two sites within the aggregate, all of the bond distances become averaged in the final crystal structure.

The unexpected encapsulation of water appears to be due to a combination of the water's strong hydrogen bonding to the aryloxy anions and its dative interactions to the surrounding potassium centers.¹² An *ab initio* study at the computationally manageable HF/6-31G* level supports this assessment. Geometry optimizations were completed on the full molecules $[(2\text{-}^t\text{Bu-C}_6\text{H}_4\text{OK})_6] \cdot (\text{diox})_6$ and $[(2\text{-}^t\text{Bu-C}_6\text{H}_4\text{OK})_6 \supset (\text{H}_2\text{O})] \cdot (\text{diox})_6$ (Scheme 5.1 and Figure 5.4). These basic calculations confirm that water encapsulation is not only feasible but is actually energetically favored over the water-free parent molecule by -14.7 kcal/mol.



Scheme 5.1 Energetics of water encapsulation for the hexameric aggregate (HF/6-31G*).

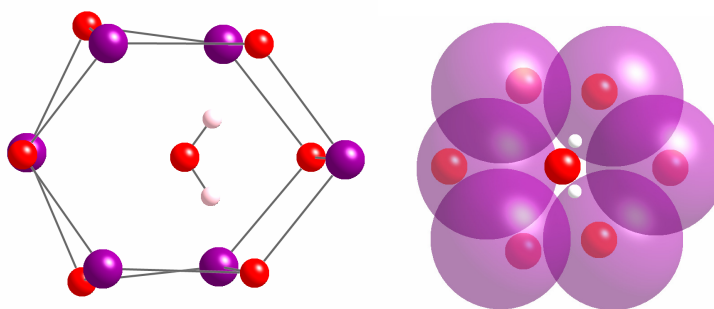


Figure 5.4 Ball and stick, and CPK space-filling views of the $[\text{K}_6\text{O}_6 \supset \text{H}_2\text{O}]$ core of the calculated structure.

5.2.3 Crystallographic and Solution Studies of **5.1**

In order to better understand the water encapsulation of **5.1** a series of crystallization reactions were performed under varying conditions. By changing the reaction conditions we hoped to either completely remove all of the water, add additional water, or replace the encapsulated water with another guest molecule. It was hoped that this study would provide a better understanding of the role of the water molecule and the overall stability of the aggregate. A summary of the reaction conditions for this study are listed in Table 5.2 along with the metrical parameters for the crystallized products.

Generally, the addition of water to alkali metal complexes will eventually result in either hydrolysis, as discussed in the introduction, or complete hydration of the metal centers. Hydrolysis is precluded in this system because of the low pK_a of the phenol (11.34 for 2-*tert*-butylphenol versus 15.75 for water).¹³ Interestingly, the deliberate addition of excess water to the reaction is needed to produce full occupancy of encapsulated water in the hexamer (*i.e.* 50% occupancy over the two disordered sites), entry **5.1**. The structure is synthesized using a 2:1 molar equiv. ratio of water to aryloxy. Moreover, the reaction of KOH with the phenol in 1,4-dioxane also produces crystals (entry **V**) despite the *in situ* generation of equimolar quantities of water.¹⁴ Therefore, the hexameric monohydrate appears to be remarkably stable to further hydration. However, using a 6:1 molar ratio of water or greater (entries **I** and **II**) in the starting reaction prevents crystallization. The large steric bulk of the *t*-butyl group on the aromatic ring undoubtedly helps in the stability of the aggregate. In the solid-state structure, as well as the calculated structure, all of the *t*-butyl groups face away from the center of the aggregate (Figure 5.3). This steric bulk located in a ring around the outside

of the aggregate may prevent the aggregate from breaking open when water is encapsulated within the cage.

TABLE 5.2

KEY BOND LENGTHS [\AA] AND WATER OCCUPANCY FOR **5.1** AND **I-XVI**

Entry	K-O _{Ar}	K-O _{H₂O}	Water Site Occupancy (%)	Synthetic Conditions
5.1	2.521(1) - 2.761(1)	2.732(2) - 2.751(2)	50.00	2 eq. H ₂ O added
I	—	—	—	6 eq. H ₂ O added
II	—	—	—	9 eq. H ₂ O added
III	2.562(2) – 2.735(2) <2.670>	2.643(7) – 2.810(7) <2.734>	29.08	Schlenk open for 15 min.
IV	2.555(2) – 2.746(2) <2.673>	2.651(7) – 2.806(7) <2.651>	33.99	Schlenk open all night
V	2.567(2) – 2.733(2) <2.668>	2.685(11) – 2.791(11) <2.752>	24.60	KOH used as base
VI	2.560(5) – 2.735(5) <2.669>	2.641(6) – 2.789(6) <2.724>	33.87	No water added
VII	2.550(2) – 2.753(2) <2.677>	2.670(6) – 2.803(6) <2.738>	41.98	From same batch as VI
VIII	2.563(3) – 2.734(3) <2.668>	2.630(11) – 2.825(11) <2.738>	26.33	Completely dry
IX	2.562(2) – 2.730(2) <2.667>	2.628(8) – 2.818(8) <2.733>	23.64	From same batch as VII
X	2.581(5) – 2.739(4) <2.687>	2.719(11) – 2.777(15) <2.754>	32.03	Reaction inside glovebox
XII	—	—	—	Molecular sieves present
XII	—	—	—	K(m) as metal source
XIII	2.558(2) – 2.724(2) <2.662>	2.614(8) – 2.822(8) <2.730>	22.97	O ₂ through dioxane
XIV	—	—	—	O ₂ through reaction
XV	2.552(1) – 2.722(1) <2.651>	2.612(15) – 2.848(15) <2.734>	5.89	Anhydrous hydrazine present
XVI	2.562(3) – 2.737(3) <2.670>	2.68(2) – 2.82(2) <2.76>	14.72	Ammonia gas through reaction

Repeated attempts to prepare an anhydrous derivative of **5.1** resulted in lower or no yield of crystals. By not adding any water to the original reaction mixture (entry **VI**

and **VII**) crystals of **5.1** formed, but the central water molecule does not have the full 50% occupancy at each of the two disordered water sites. This indicates that during crystal formation there is a mixture of aggregates, only some of which contain an encapsulated water molecule. The use of meticulously dried and degassed reagents, solvents and glassware resulted in the formation of crystals with an even lower occupancy of water (entry **VIII** - **X**). Attempts to remove the water from the reaction using molecular sieves (**XI**) or potassium metal (**XII**) resulted in no crystal formation. These results suggest that at least a small amount water actually needs to be present in order for **5.1** to crystallize.

Attempts to replace the encapsulated water with other small molecules produced either no crystalline material or only the encapsulated water complex. These attempts included using oxygen (**XIII** and **XIV**), hydrazine (**XV**), and ammonia (**XVI**). The ability of water to act as a hydrogen bond donor and a Lewis base donor, coupled with its small size, may give the hexameric aggregate significantly increased stability compared with other comparable small molecules like ammonia. Although the hydrazine and ammonia are not encapsulated, they crystallize as **5.1** with by far the lowest percentage of encapsulated water. Instead of becoming encapsulated they may be acting as *in situ* drying reagents to remove any available water.

In order to better understand the effect water has on the system, a NMR water addition experiment in THF- d_8 was carried out on **5.1** (Figure 5.5). Although X-ray crystallography clearly indicates the presence of encapsulated water, no water is seen initially in the NMR spectrum (Figure 5.5a). Moisture was slowly added to the system by opening the NMR tube to the air, and then recollecting the spectrum after 5 minutes. A

broad water peak appears at 6.08 ppm upon the first addition of moisture (Figure 5.5b) and integrates to slightly more than $\frac{1}{2}$ water molecule per hexamer. Addition of more moisture (Figure 5.5c) shows a downfield shift in the water peak (to 6.15 ppm) as well as an increase to 1.5 water molecules per hexamer. Upon letting the NMR sample sit for 24h the water peak is shifted *upfield* to 5.81 ppm (Figure 5.5d). The initial downfield shift of the water peak followed by an upfield shift will be seen later in the potassium 2-isopropylphenoxide dioxane system (Figure 5.15). During water addition, all of the aromatic hydrogens move downfield, although the largest change is in the *ortho*-hydrogen. When no water is present the peak is at 6.24 ppm, but eventually shifts downfield to 6.37 ppm (Figure 5.5d).

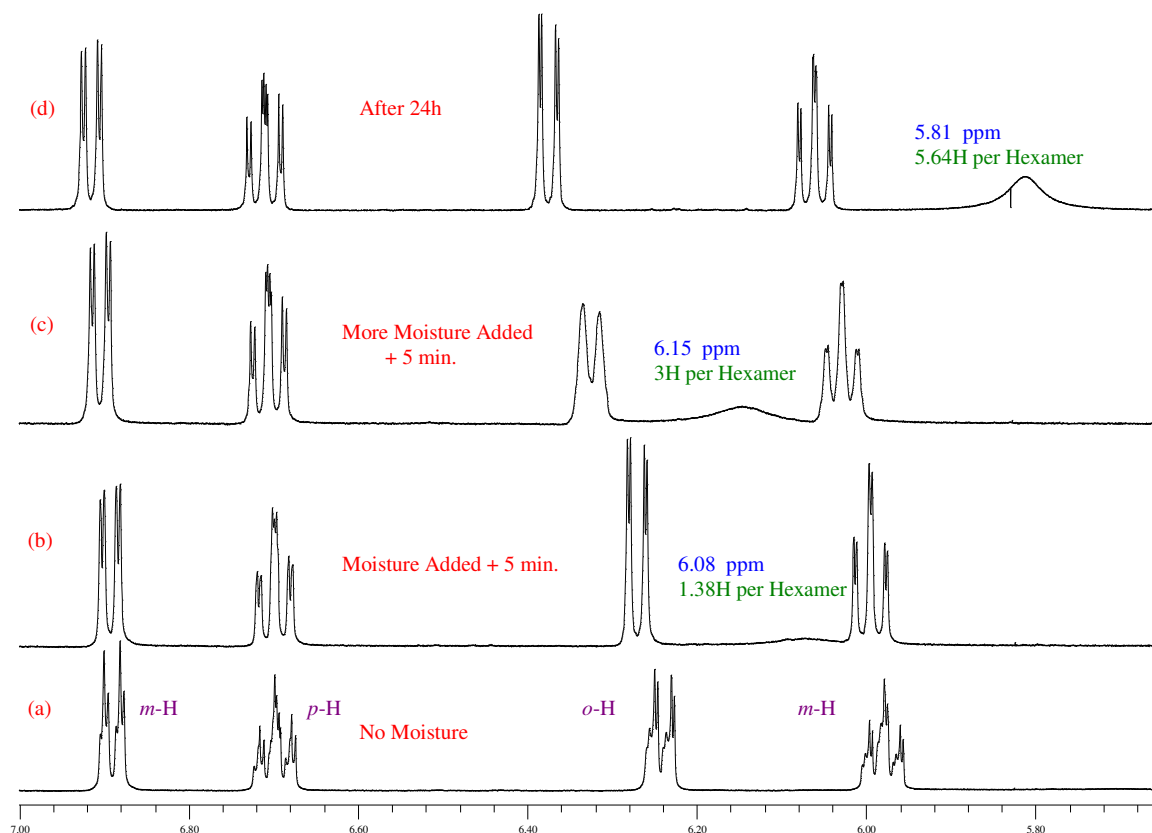


Figure 5.5 Water addition to **5.1** in THF- d_8 .

5.2.4 Extended Structure of Potassium 2-*tert*-Butylphenoxide Dioxane

While the molecular structure of **5.1** is fascinating because of the ability of the aggregate to encapsulate water, the extended structure is relatively unremarkable in terms of connectivity. The hexameric aggregate is coordinated by six dioxane molecules. Two of the dioxanes terminally bind to the aggregate, while the remaining four dioxanes bridge to neighboring hexamers, leading to formation of a two-dimensional 4^4 -net (Figure 5.6). The terminal dioxanes have a K-O_{diox} bond distance of 2.606(2) Å, while the bridging dioxanes have slightly longer bond distances of 2.616(2) Å and 2.619(2) Å. The centroid-centroid distance between aggregates is 12.758 Å.

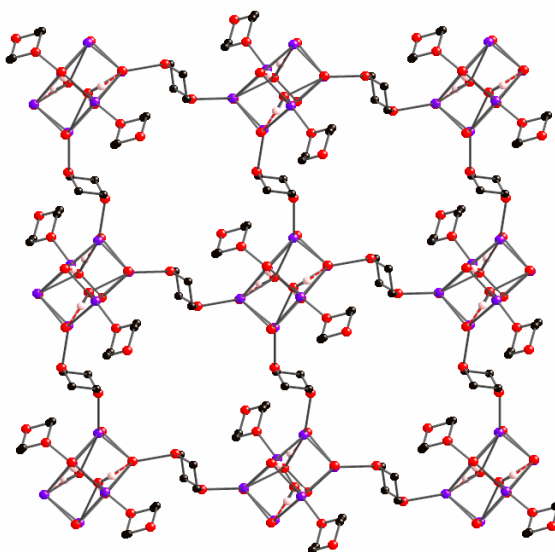


Figure 5.6 The extended two-dimensional 4^4 -net of **5.1_n** resulting from four bridging and two terminal dioxane molecules per hexameric aggregate.

5.2.5 Characterization of Potassium 2-*tert*-Butylphenoxide THF

Due to the unique ability of **5.1** to encapsulate water, we wished to test the robustness of the system by systematically changing the reaction variables. The first variable we studied was the effect of solvation on the aggregate. We reasoned that as long

as the hexameric aggregate is retained, replacement of the dioxane with another solvate should not influence the ability of the aggregate to encapsulate water. The THF solvate of **5.1** has previously been published in a study of potassium aryloxides.¹⁵ The structure is very similar to **5.1** in that it forms a hexameric drum aggregate where each of the potassiums are coordinated by one molecule of THF. There is no mention of the published structure having a water molecule encapsulated within the aggregate. However, a careful review of the CIF file reveals a large residual electron peak of 2.42 e⁻ in the Fourier map that is unaccounted for in the published work.

In order to better understand the structure, we grew high quality crystals of the THF solvate, $[\{(2\text{-}t\text{Bu-C}_6\text{H}_4\text{OK})_6\supset(\text{H}_2\text{O})\} \cdot (\text{THF})_6]$ (**5.2**), from a THF / hexane solution. Single crystal X-ray diffraction of **5.2** gives the same structure as seen in the literature, but with a large *q*-peak within the aryloxide cage. Similar to **5.1**, the most reasonable assignment for this site is the oxygen of a water molecule. Symmetry expansion through the crystallographic inversion center leads to a pair of water molecules, each with a partial occupancy of ~50% (Figure 5.7).

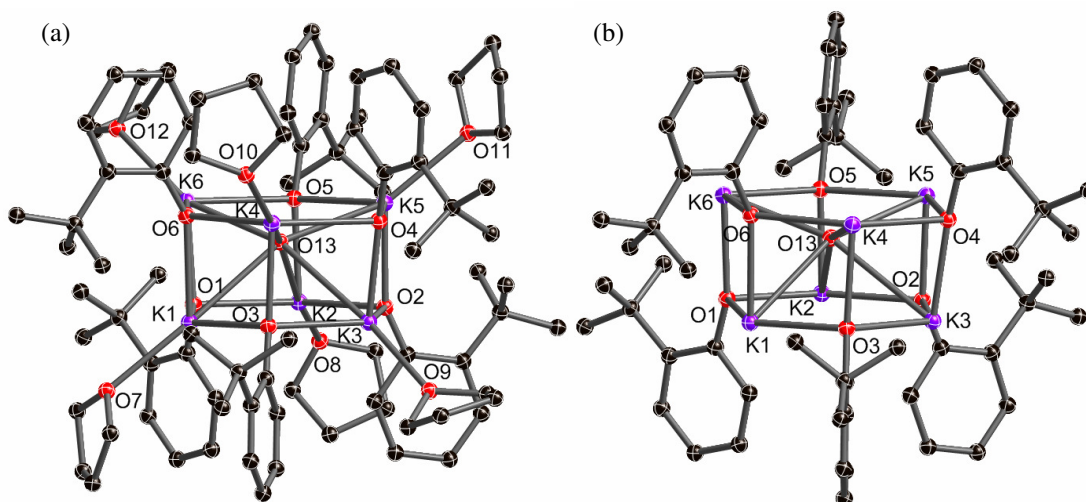


Figure 5.7 Structure of $[\{(2\text{-}t\text{Bu-C}_6\text{H}_4\text{OK})_6\supset(\text{H}_2\text{O})\}\cdot(\text{THF})_6]$, **5.2**, showing (a) the full hexameric aggregate with one of the water sites, and (b) the prismatic hexamer highlighting one water site within the aggregate, with non-water hydrogens and dioxanes removed for clarity.

As expected, the metrical parameters of **5.2** are similar to **5.1**. The average M-O_{Ar} distance in both structures is within 0.05 \AA and the average M-O_{THF} distance in **5.2** is only 0.08 \AA longer than the average M-O_{diox} distance in **5.1**. The water molecule in **5.2** sits slightly closer to the center of the cage with a distance of 0.80 \AA between the oxygen and the hexameric K_3O_3 plane whereas the distance in **5.1** is 0.68 \AA . There are two short $\text{O}_{\text{H}_2\text{O}}\text{-O}_{\text{Ar}}$ distances of 2.628 and 2.673 \AA as well as one long distance of 3.205 \AA , similar to **5.1**, indicating a set orientation of the water within the aggregate.

5.2.6 Structure of Rubidium and Sodium 2-*tert*-Butylphenoxide Dioxane

In order to further understand the ability of this system to encapsulate water, we looked at the rubidium and sodium analogues of **5.1**. As long as the hexameric aggregate remains intact, the larger and smaller metals will help test the limits of water encapsulation. High quality crystals of both analogues, $[\{(2\text{-}t\text{Bu-C}_6\text{H}_4\text{ORb})_6\supset(\text{H}_2\text{O})\}\cdot(\text{dioxane})_4]\cdot(\text{dioxane})]_{\infty}$ (**5.3**) and $[\{(2\text{-}t\text{Bu-}$

$\text{C}_6\text{H}_4\text{ONa})_6\supset(\text{H}_2\text{O})\}\cdot(\text{dioxane})_3]_\infty$ (**5.4**) were grown from a dioxane solution. Both structures form the targeted water encapsulated prismatic hexamers that are coordinated by dioxane.

Similar to **5.1** and **5.2**, there is a water molecule that is disordered over two sites in the rubidium analogue **5.3** (Figure 5.8). Because of symmetry, each water site is 0.627 and 2.210 Å away from the two Rb_3O_3 faces of the aggregate. In the two previous compounds, the water was essentially equidistant to the three potassiums in each face. However, there is always two short and one long $\text{O}_{\text{H}_2\text{O}}\text{-O}_{\text{Aryl}}$ distance. The neutron data of **5.1_n** showed that this is due to the strong hydrogen bonding of the water molecule. This effect is also seen in **5.3**. The three $\text{Rb-O}_{\text{H}_2\text{O}}$ bond distance falls into a narrow range of 2.91(2) – 2.96(2) Å, but there are two short O-O bond distances of 2.66 ($\text{O}_1\text{-O}_8$) and 2.51 Å ($\text{O}_3\text{-O}_8$), as well as one long distance of 3.52 Å ($\text{O}_2\text{-O}_8$). Although the hydrogen atoms of the water in **5.3** cannot be detected using X-ray diffraction, this is a clear indication that the water molecule has a set orientation. Interestingly, there is no elongation of one metal thermal ellipsoid as seen in **5.1**.

Although the frequent formation of large aggregates might be expected for rubidium complexes, this is not the case. In fact there are only three examples of tetrameric rubidium aggregates¹⁶ and only one example of a hexameric rubidium aggregate in the literature.¹⁷ As briefly discussed in the previous chapter for the cesium complex (**4.7**), the heavier alkali metal complexes tend to form unsolvated polymeric complexes rather than discreet solvated complexes. The large 2-*tert*-butyl substituent in **5.3** has a stabilizing influence over the complex to give only the second example of a hexameric rubidium aggregate. Although there are not a lot of comparable structures, the

Rb-O_{Ar} distances in **5.3** of 2.781(2) – 3.036(3) Å are similar to the Rb-O_{Ar} distances seen in the dimeric and pentamer aggregates (**4.5**, **4.6**, and **4.9**) discussed in the previous chapter.

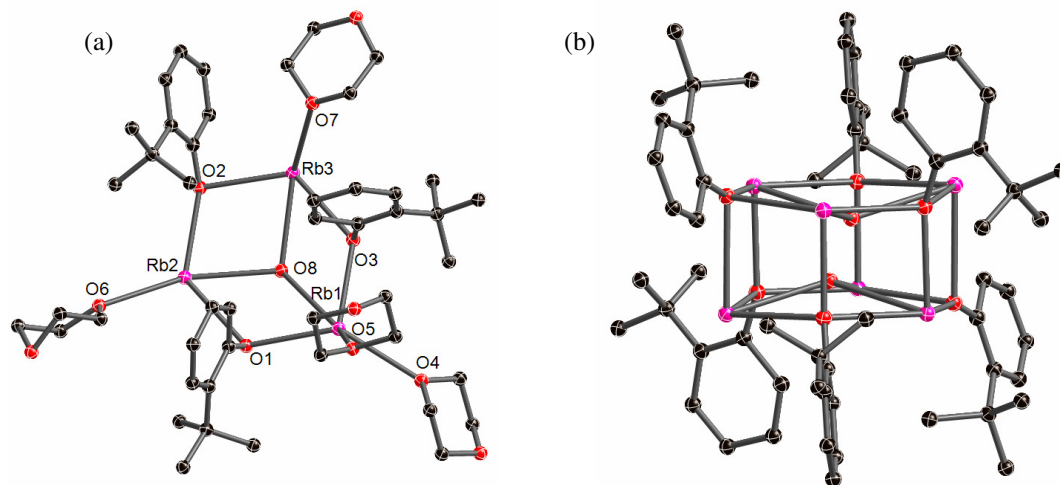


Figure 5.8 Structure of **5.3**, showing (a) the asymmetric unit with the encapsulated water molecule, and (b) the prismatic hexamer highlighting both of the water sites within the aggregate with hydrogens and dioxanes removed for clarity.

The molecular structure of the sodium analogue, **5.4**, is very similar to **5.1-5.3**. The hexameric aggregate is coordinated by six dioxanes with an encapsulated water molecule that is disordered over two sites (Figure 5.9). Each water site lies 0.418 and 1.851 Å away from the two Na₃O₃ faces of the aggregate. Because of crystallographically imposed symmetry, the central water molecule has the same bond distance to all three sodiums. As expected from the previous structures, the Na-O_{H2O} distance of 2.360(6) Å is nearly identical to the average Na-O_{Ar_{yl}} distance of 2.378 Å (range is 2.277(1) – 2.440(1) Å). The Na-O_{Diox} distance of 2.360(6) is also similar to the distances previously reported by our group for dioxane solvated sodium aryloxides.^{1b}

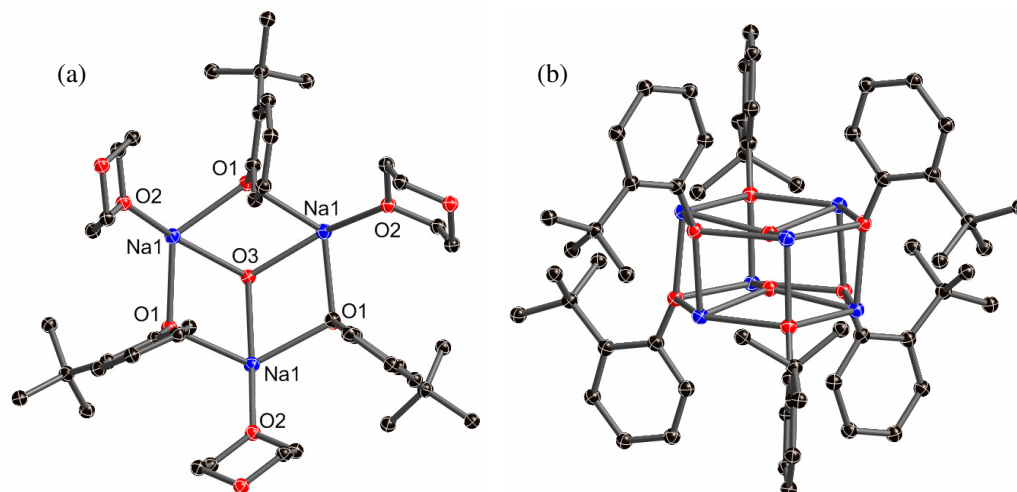


Figure 5.9 Structure of **5.4**, showing (a) half of the hexameric aggregate with encapsulated water molecule, and (b) the prismatic hexamer highlighting both of the water sites within the aggregate, with hydrogens and dioxanes removed for clarity.

Unlike the encapsulated water in **5.1-5.3**, the water molecule in **5.4** has the same bond distance to all of the aryl oxygen atoms (2.557 Å), likely indicating the water has no set orientation inside the aggregate. Interestingly, this suggests that the water in the small sodium aggregate is not in a clearly defined orientation, as was found for the larger potassium and rubidium aggregates.

All of the dioxanes in both **5.3** and **5.4** bridge to other aggregates to form an 8- and 6-connected networks, respectively. The 8-connected network of **5.3** adopts the highest possible symmetry for its connectivity, which is the body-centered cubic (**bcc**) net (Figure 5.10). The **bcc** net was previously seen for the pentameric rubidium 2,4,6-trimethylphenoxide complex (**4.10**) described in the previous chapter. Unlike the extended structure of **4.10** which is formed through the combination of single and double dioxane bridges, the extended network of **5.3** is connected through only single bridges.

Although 8-connected networks are still relatively rare in coordination networks, the high-symmetry **bcu** topology is clearly the most favored.¹⁸

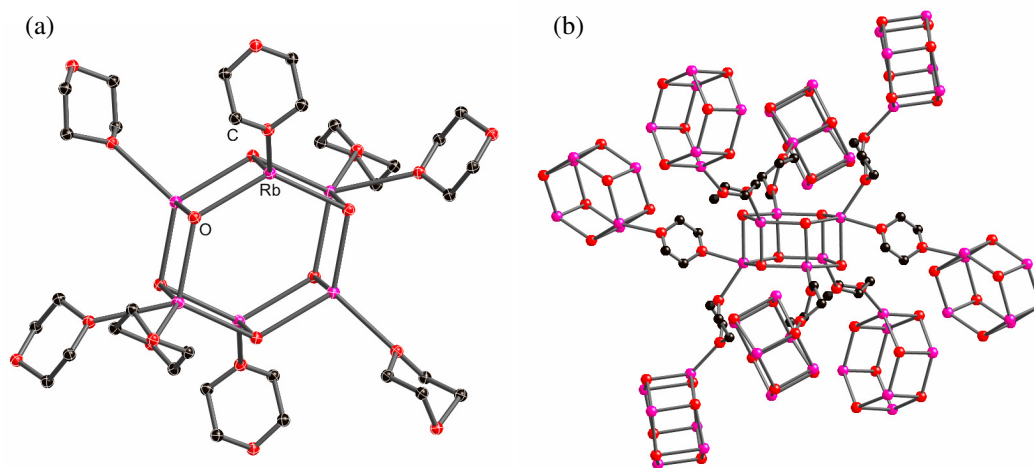


Figure 5.10 (a) The prismatic hexamer **5.3** highlighting the eight coordinated dioxanes, and (b) the eight linked aggregates that form part of the extended three-dimensional network with **bcu** topology. Hydrogen atoms and the carbon atoms of the aryloxides are removed for clarity.

The six dioxanes that coordinate to each aggregate in **5.4** form single bridges to other aggregates to give the common primitive cubic (**pcu**) topology (Figure 5.11). The **pcu** topology is not only common for octahedrally coordinated transition metals, but was seen regularly in previous work by our group using sodium aryloxide aggregates to synthesis extended networks.^{1b} Looking at the entire metal series for this system (**5.1**, **5.3**, and **5.4**) it is unsurprising that the sodium and potassium analogues have six coordinated dioxanes per aggregate and the larger rubidium has eight. Interestingly though, all of the dioxanes in the sodium aggregate bridge to give a 3D network but only four bridge in the larger potassium aggregate to give a 2D network. As was seen in our group's previous work using lithium and sodium aryloxides, even the smallest change in the size of the localized structure can strongly influence the resulting topology of the extended structure.

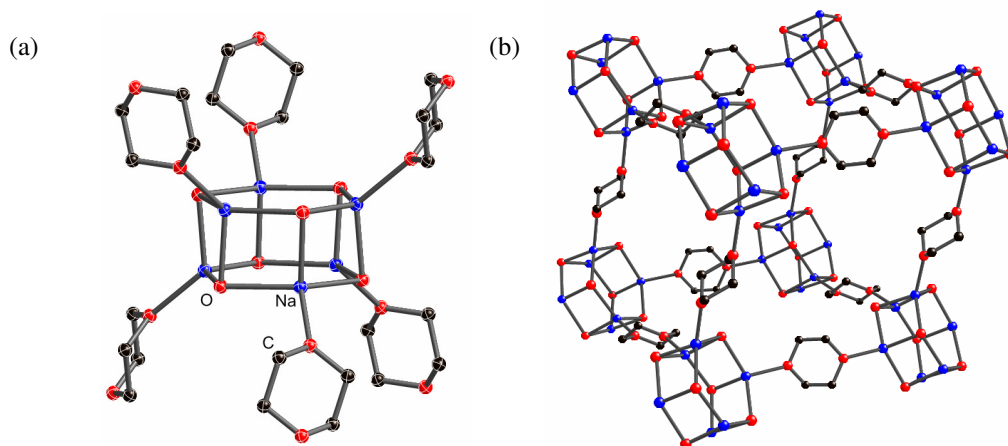


Figure 5.11 (a) The prismatic hexamer **5.4** highlighting the six coordinated dioxanes, and (b) the six linked aggregates that form part of the extended three-dimensional network with **pcu** topology. Hydrogen atoms and the carbon atoms of the aryloxides are removed for clarity.

5.3 Reactions of 2-Isopropylphenol

5.3.1 Synthesis

To determine if water encapsulation is specific to the 2-*tert*-butylphenol ligand or a more general phenomenon for this class of compounds, the closely-related ligand 2-isopropylphenol was studied. Subsequently, the potassium complex $[\{(2\text{-}^i\text{Pr-C}_6\text{H}_4\text{OK})_6 \supset \text{H}_2\text{O}\} \cdot (\text{diox})_5] \cdot (\text{diox})]_\infty$, **5.5**, was successfully prepared and its structure elucidated by single-crystal X-ray diffraction. The subtle change of *tert*-butyl to *isopropyl* also critically alters the sensitivity of the system to hydration. As such, we were able to prepare the water-free complex, $[(2\text{-}^i\text{Pr-C}_6\text{H}_4\text{OK})_6 \cdot (\text{diox})_5]_\infty$ (**5.6**), as well as the dihydrated complex, $[\{(2\text{-}^i\text{Pr-C}_6\text{H}_4\text{OK})_6 \cdot (\text{H}_2\text{O})_2\} \cdot (\text{diox})_{5.5}]_\infty$, (**5.7**). Finally, we were able to prepare the rubidium complex, $[(2\text{-}^i\text{Pr-C}_6\text{H}_4\text{ORb})_6 \cdot (\text{diox})_{4.5}]_\infty$ (**5.8**), to give a more complete understanding of the isopropylphenoxide series. All of the compounds were

synthesized by the equimolar reaction of 2-isopropylphenol with either KHMDS or $[\text{RbOBu}^t\cdot\text{Bu}^t\text{OH}]_\infty$ in dioxane.

5.3.2 Molecular Structures of Potassium 2-Isopropylphenoxide Dioxane

The aggregated structure of **5.5** is essentially identical to **5.1**, with water again encapsulated within the prismatic K_6O_6 hexamer (Figure 5.12). The water is disordered over two sites with a distance of 0.956 Å to the nearest K_3O_3 face. This is nearly 0.3 Å longer than in **5.1**, although the mean $\text{K}-\text{O}_{\text{H}_2\text{O}}$ distance of 2.828 Å (range of 2.779(11) – 2.876(11) Å) is nearly the same. In contrast to **5.1** – **5.3**, there is not two short and one long $\text{O}_{\text{H}_2\text{O}} - \text{O}_{\text{Ar}}$ distance. This suggests that the water molecule is most likely rotationally disordered. Evidence of this rotational disorder can also be seen in the elongation of the thermal ellipsoids of all six potassium centers. In contrast, only one potassium (and its symmetry equivalent) has an elongated ellipsoid in **5.1**. This suggests that the water in **5.5** is disordered over all six possible binding sites, which is likely a consequence of the smaller isopropyl groups allowing more flexing of the structure.

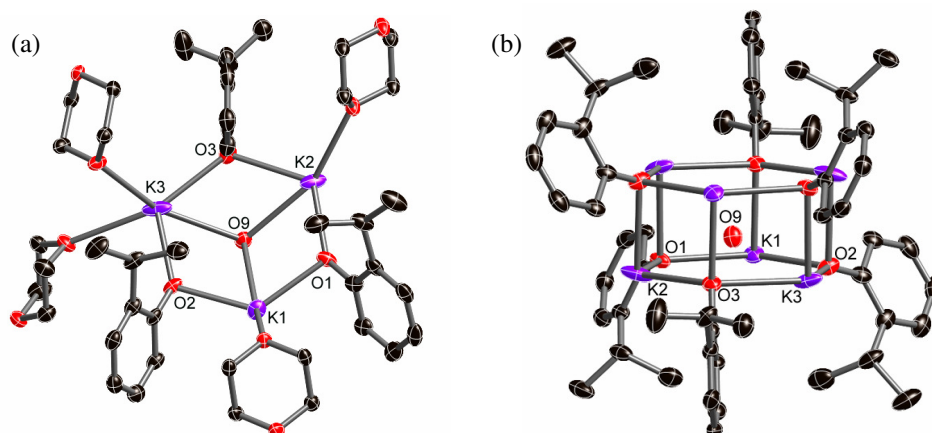


Figure 5.12 Structure of **5.5**, showing (a) the asymmetric unit with hydrogen atoms removed for clarity, (b) the prismatic hexamer highlighting one of the water sites within the aggregate. The six dioxane molecules are removed for clarity.

Pleasingly, using this system we were able to prepare the water-free derivative $[(2\text{-}^i\text{Pr-C}_6\text{H}_4\text{OK})_6\cdot(\text{diox})_5]_\infty$, **5.6**, which was structurally characterized, and is shown in Figure 5.13. The most striking feature of **5.6** is that a hexameric aggregate is found again but it now adopts a compact ‘triple-stack of dimers’ motif.¹⁹ Interestingly, both prismatic hexamers and triple-stacks of dimers have previously been reported for alkali metal aryloxides.¹⁹ However, little rationalization has appeared to explain why both structural isomers appear. Retention of hexameric aggregation in **5.5** and **5.6** clearly illustrates the stability of this arrangement for these metal-ligand-solvent systems. Incorporation of water only requires opening of the two central K-O_{Ar} contacts in **5.6** to give the prismatic isomer. The K-O_{Ar} mean bond distance in **5.6** is 2.733 Å, with a range of 2.559(1) – 2.944(1) Å. These distances are moderately longer than those seen in the prismatic hexamer of **5.5** with a mean of 2.670 and a range of 2.568(1) – 2.792(3). This suggests that as the “collapsed” triple-stack of dimers is formed to maximize bonding, the steric bulk of the ligand, in combination with the higher coordination number of the middle potassium centers, forces some elongation of the bonds.

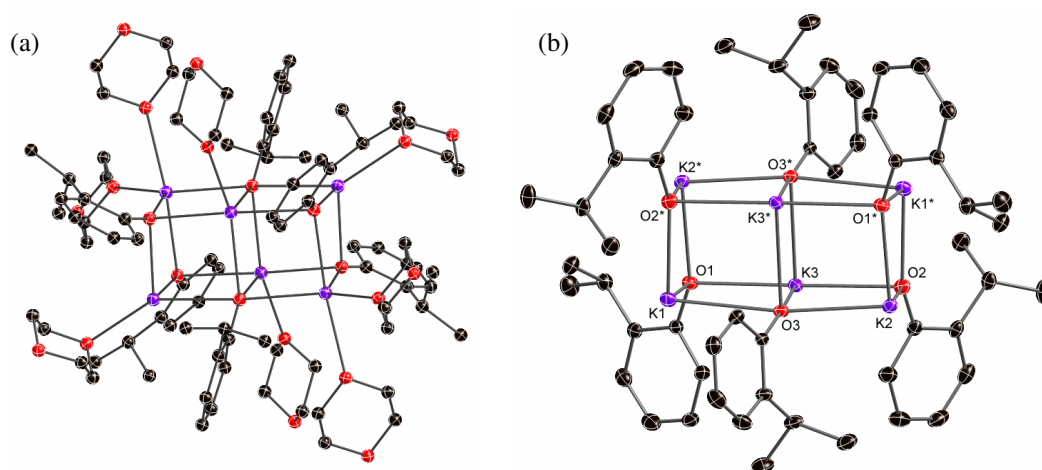


Figure 5.13 The water-free hexameric aggregate of **5.6** with dioxane molecules and hydrogens removed for clarity.

Although the extended structures are discussed later, both of the hexameric aggregates in **5.5** and **5.6** are coordinated by eight dioxane molecules. The K-O_{Diox} distances are hardly perturbed in going from the open prismatic hexamer to the closed triple-stack of dimers aggregate, with a mean distance of 2.769 and 2.718 Å in **5.5** and **5.6**, respectively. In both structures there are a total of six bridging and two terminal dioxanes. In **5.5** the two terminal dioxanes coordinate to potassium centers that are also coordinated by a bridging dioxane. In **5.6** the arrangement is slightly different, with the two central potassium atoms of the aggregate coordinated by only the two terminal dioxanes. This leaves the outer four potassiums coordinated by the six bridging dioxanes.

The subtle change of *tert*-butyl to isopropyl critically alters the sensitivity of the system to hydration. Increasing the molar ratio of water to aryloxide from 1:6, used to prepare **5.5**, to 2:6 allows the isolation of the dihydrate [$\{(2\text{-}^i\text{Pr-C}_6\text{H}_4\text{OK})_6\cdot(\text{H}_2\text{O})_2\}\cdot(\text{diox})_{5.5}\}_\infty$, **5.7** (Figure 5.14). The crystal structure of **5.7** again consists of linked hexameric units consistent with **5.1-5.6**, but now the additional water breaks open an edge of each K₃O₃ ring, where K6-O6 is 3.695, K1-O3 is 4.652 Å, and the remaining K-O_(Ar) distances are <3 Å. An additional interesting feature of the bonding within the aggregate is that the oxygen of one of the bridging dioxane molecules, O(8), acts as a μ -bridge between two potassium atoms. This is the first example of dioxane coordinating to metals in this fashion, although it has been well documented for THF (77 known structures in the CSD).²⁰

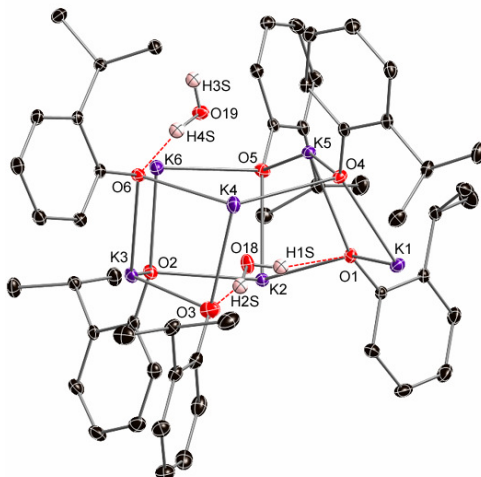


Figure 5.14 The dihydrated hexameric aggregate of **5.7** highlighting the one water molecule encapsulated within the aggregate and the second water molecule coordinated on the outer face. Dioxane molecules and non-water hydrogen atoms are removed for clarity.

One of the water molecules can still be considered to be within the loose cage, with O18 lying 0.14 Å above the closest K_3O_3 mean plane. This water again hydrogen bonds to a pair of aryloxide anions and interacts with two potassium centers (K3-O18 is 2.788(1) and K2-O18 is 2.883(1) Å). The second water sits 1.50 Å out of the closest K_3O_3 mean plane, forming two dative interactions K6-O19 at 2.727(1) and K5-O19 at 2.807(1) Å. Since it is no longer encapsulated, this second water molecule forms only a single hydrogen bond to an aryloxide, with the remaining hydrogen directed towards a dioxane molecule of a neighboring cage (H3s-O10 is 2.018(2) Å, O19-H3s-O10* is 170.53(2)°).

5.3.3 Solution Studies of Potassium 2-Isopropylphenoxide Dioxane

Solution NMR studies were carried out in d_2 -methylene chloride for **5.5** - **5.7** to better understand the solution behavior of the complexes, as well as the effects water

addition has on the system. These complexes proved amenable to solution studies since the zero, one, and two water complexes are all characterized in the solid state. Particularly revealing is the comparison between the water-free complex, **5.6**, and the two-water complex, **5.7**.

As shown in Figure 5.15, very small amounts of water can be added to the water-free complex **5.6** and quantitatively measured by ^1H NMR. Immediately noticeable is the small water peak that begins to appear at 6.68 ppm in Figure 5.15b. Integration of the peak shows there is 1.1 hydrogen atoms per hexamer, which equates approximately to one-half water. Addition of water causes a downfield shift of the water (Figure 5.15c-d), and then a shift back upfield to 6.68 ppm (Figure 5.15e-f) during which the relative size of the water peak increases. The shift downfield then back upfield has been seen previously with the *tert*-butylphenoxide derivative **5.1**. The water peak in Figure 5.15e integrates to 4.3 hydrogen atoms, which is slightly more than two water molecules per hexamer. The addition of water has the most pronounced effect on the *ortho*-hydrogen of the aromatic ring. In the water-free complex the doublet comes at 6.20 ppm (Figure 5.15a), but upon addition of water the doublet begins to broaden and shift downfield until it reaches 6.32 ppm (Figure 5.15f). The rest of the aromatic hydrogen atoms shift downfield by less than 0.04 ppm during the entire course of water addition.

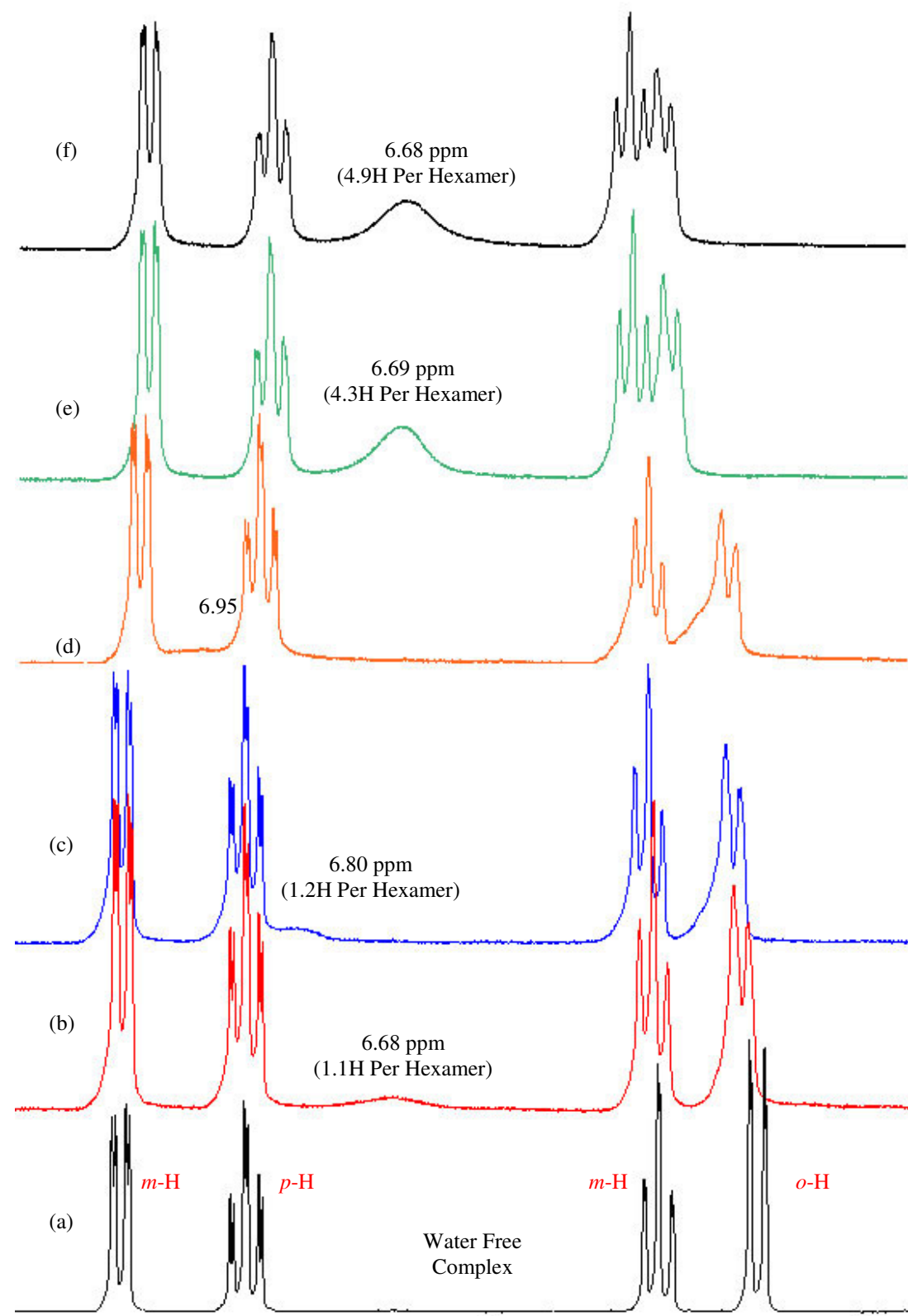


Figure 5.15 Water addition to 5.6 in CDCl_2 .

The aromatic region of the two-water complex **5.7** is shown in Figure 5.16. The water peak at 6.62 ppm integrates as exactly two water molecules per hexamer. The peak positions in this complex highly resembles that of Figure 5.15e, in which the equivalent of two water molecules per hexamer were added. The major difference is the water peak in Figure 5.15e is broader, suggesting a more dynamic solution equilibrium.

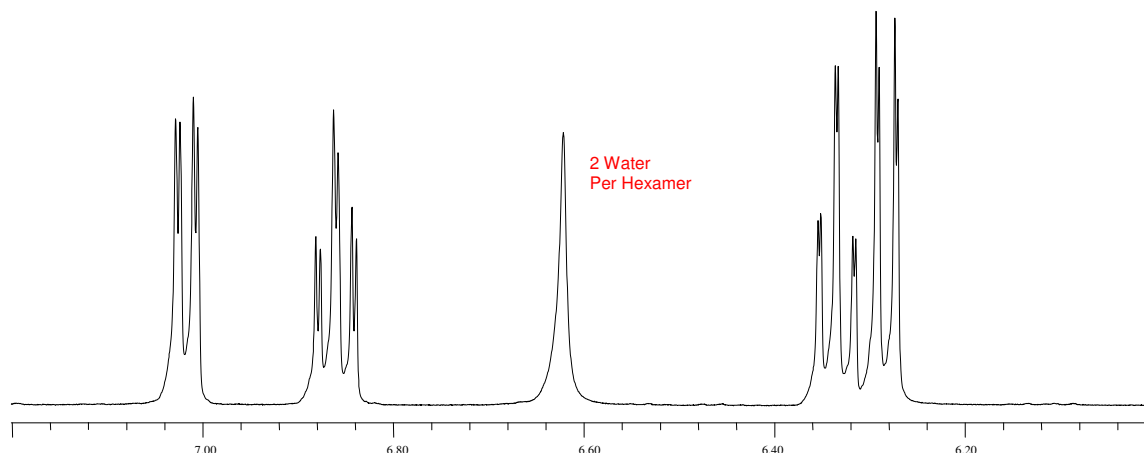


Figure 5.16 Aromatic region of **5.7** in CD_2Cl_2 .

A variable temperature ^1H NMR study in d_2 -methylene chloride was run for complex **5.7**, as shown in Figure 5.17. Complex **5.7** was chosen for this study since **5.5** and **5.4** have low solubilities in CD_2Cl_2 . The most noticeable change in the spectrum is the downfield shift of the water peak going from room temperature (Figure 5.17a) to -75°C (Figure 5.17g). The water peak starts at 6.76 ppm at room temperature, and then shifts downfield to 7.49 ppm at -40°C , during which it also begins to broaden. Below -40°C the water peak cannot be seen because it is too broad (Figure 5.17f,g). It can also be seen in Figure 5.17 the upfield shift and broadening of all of the aromatic hydrogens during cooling. The most noticeable shift is in the *ortho*-hydrogen, which shifts from 6.25 ppm at room temperature to 6.16 ppm at -75°C . After cooling, the NMR sample was rewarmed to -10°C to verify the same spectrum being present as when the sample was

initially cooled to -10 °C (Figure 5.17c). Finally, the sample was warmed to 35 °C (not shown), which showed the water peak had shifted *upfield* with respect to the room temperature sample to 6.47 ppm, which further shows the dynamic equilibrium occurring.

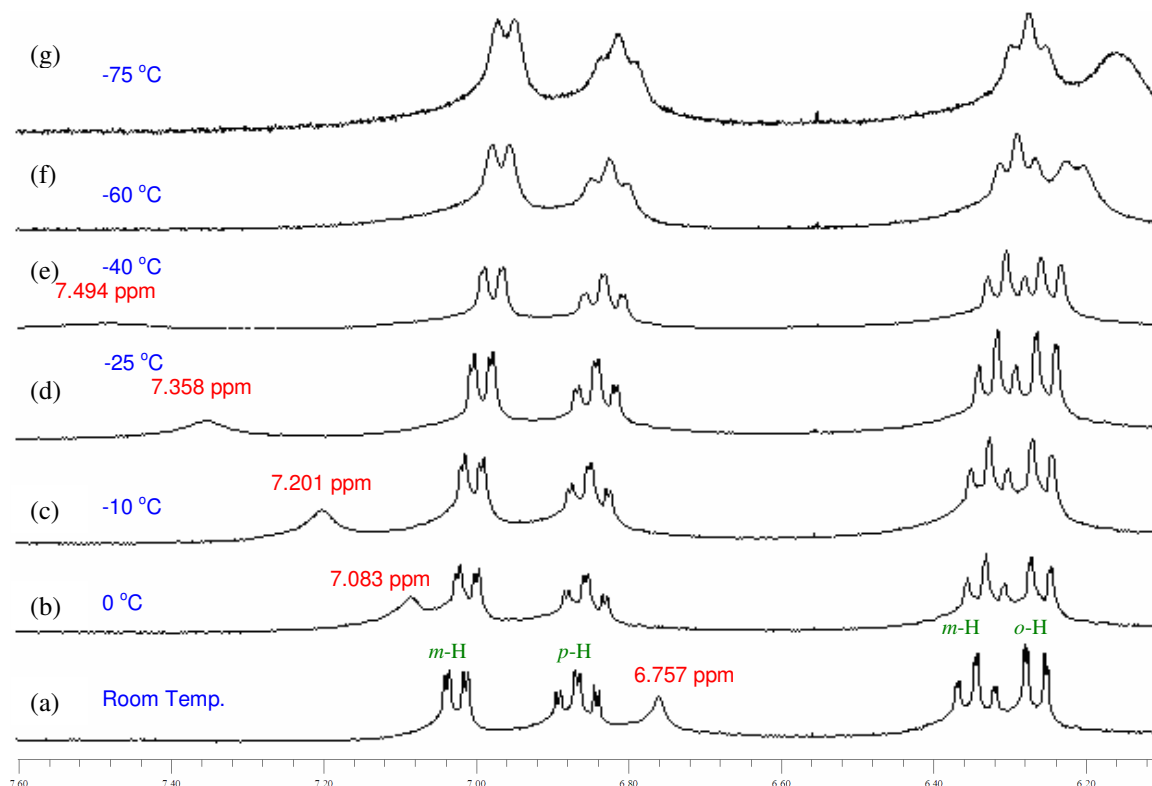


Figure 5.17 Variable temperature study of **5.7** in CD_2Cl_2 .

5.3.4 Extended Structures of Potassium 2-Isopropylphenoxide Dioxane

Compared to **5.1**, the smaller isopropyl groups of **5.5** and **5.6** now allow for the coordination of eight dioxanes to the aggregate. In **5.5**, two of the dioxanes bond terminally to the cage, leaving six dioxanes to bridge to neighboring aggregates to form a 3D primitive cubic (**pcu**) network (Figure 5.18). The structure is porous with one free molecule of dioxane per hexameric aggregate within the extended channels.

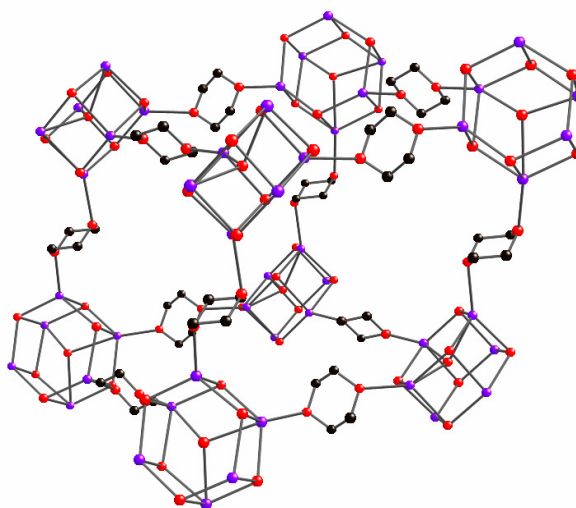


Figure 5.18 The extended three-dimensional network of **5.5** with primitive cubic topology resulting from six bridging and two terminal dioxane molecules per hexameric aggregate.

The extended structure of **5.6** is also a 3D network with the same **pcu** topology as **5.5** but without the enclathrated dioxane solvent (Figure 5.19). The average distance between centroids of the hexamer aggregates in **5.6** is 13.883 Å, which is slightly longer than the distance in **5.5** of 13.469 Å. The slight expansion of the extended structure upon guest removal has been seen before in networks synthesized by our group.²¹

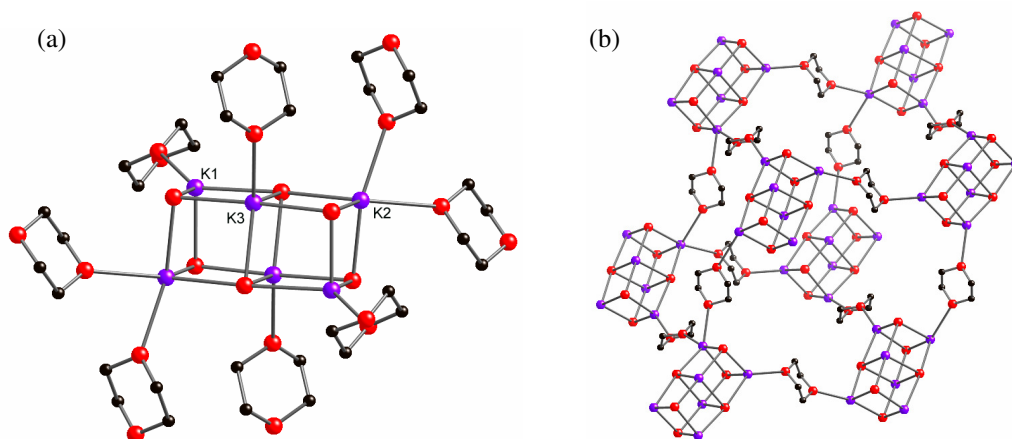


Figure 5.19 (a) The hexameric triple stack of dimers of **5.6** highlighting the eight coordinated dioxane and (b) the extended three-dimensional network with **pcu** topology resulting from six bridging and two terminal dioxane molecules per hexameric aggregate. Hydrogen atoms and the carbon atoms of the aryloxides are removed for clarity.

The extended structure of **5.7** is interesting, adopting an 4^4 -net bilayer that is connected through dioxane pillars (Figure 5.20). Although not as rare as the unique (3,4)-connected $(6^3),(6^6)$ -net bilayer reported for **3.7**, bilayers derived from pairs of 4^4 -nets are still an infrequent occurrence.²²

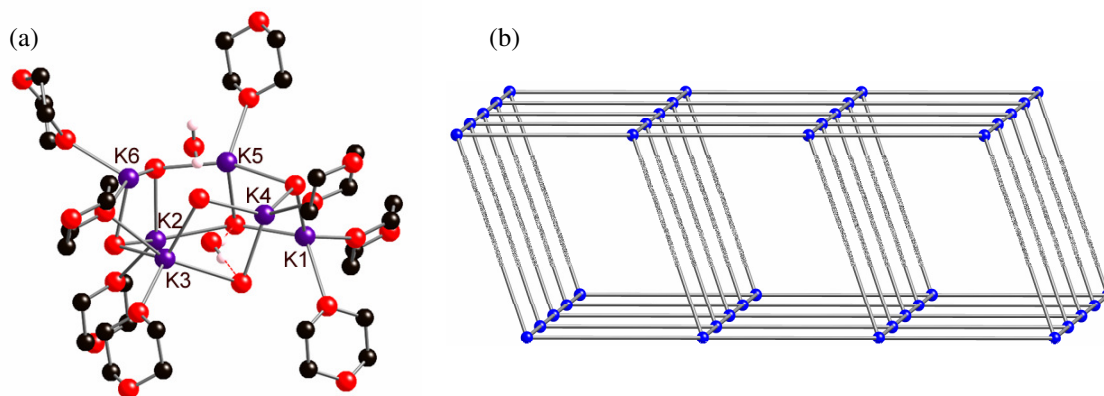


Figure 5.20 (a) Hexameric aggregate of **5.7** highlighting the eight coordinated dioxane. The carbon atoms of the aryloxy backbone are removed for clarity. (b) The extended two-dimensional bilayer structure resulting from five bridging and three terminal dioxane molecules per hexameric aggregate. The blue spheres represent the centroid of the hexameric aggregate.

5.3.5 Structure of Rubidium 2-Isopropylphenoxide Dioxane

The solid state structure of the rubidium 2-isopropylphenoxide analogue $[(2\text{-}^i\text{Pr-C}_6\text{H}_4\text{ORb})_6 \cdot (\text{diox})_{4.5}]_\infty$ (**5.8**) is remarkable, being composed of hexameric rubidium aryloxy aggregates that are coordinated by nine dioxane molecules (Figure 5.21). Similar to **5.6**, there is no water encapsulated in the aggregate.

There are three different rubidium bonding environments within the hexameric aggregate. Three of the four rubidium atoms at the two ends of the aggregate are each coordinated by two dioxane molecules, with the fourth rubidium coordinated by only one dioxane. In addition, the two central rubidium atoms are each coordinated by only one dioxane. Both the Rb-O_{Ar} and $\text{Rb-O}_{\text{Diox}}$ bond distances are similar to the rubidium 2-tert-butylphenoxide structure, **5.3**.

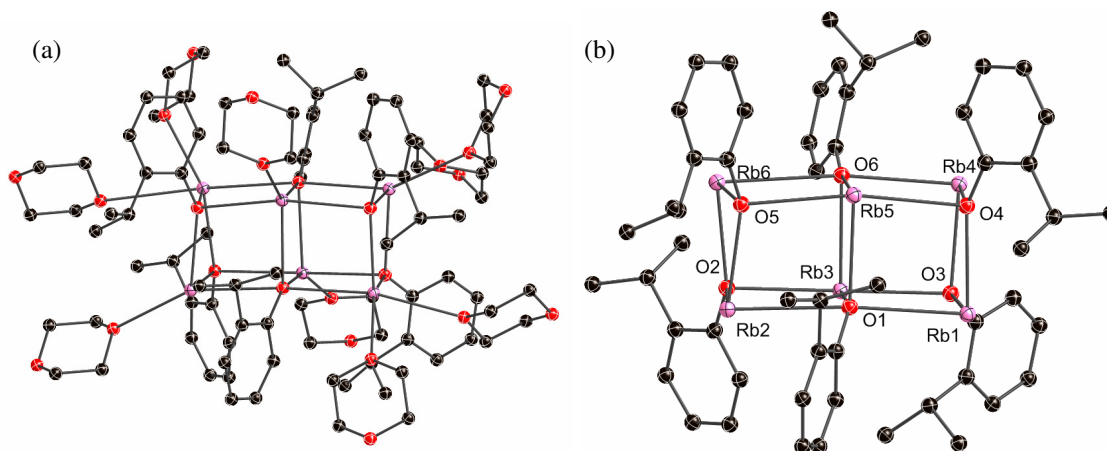


Figure 5.21 Structure of **5.8**, showing (a) the full hexameric aggregate with hydrogen atoms removed for clarity, and (b) a simplified view of the aggregate with the nine dioxane molecules and hydrogen atoms removed for clarity.

All nine of the dioxanes bridge to unique neighboring hexamers to give a 9-connected network. To the best of our knowledge this is the first uninodal 9-connected framework to be reported. We are aware of three recent reports of binodal (3,9)-

connected networks, as well as a trinodal (4,5,9)-connected network.²³ As the first true 9-connected net, **5.8** is unique because not only does it have a unique topology, but it has a completely unique connectivity.

The underlying topology of the network has a Schläfli symbol of $3^6.4^{22}.5^8$ (td10=3010) and is identified by the code **ncd** in the RCSR database. Figure 5.22 shows the overall connectivity, which is composed of parallel sheets of 4^4 -nets that are doubly intersected by $(3.4^3)(3^2.4^3)$ -nets. The complex $(3.4^3)(3^2.4^3)$ -subnets are best described by their tiling pattern, rows of squares that alternate with rows of mixed triangles and squares. The intersecting $(3.4^3)(3^2.4^3)$ -nets are offset from one another so that between each 4^4 -net layer there is an alternating pattern of rows of squares and rows of mixed triangles and squares. the two $(3.4^3)(3^2.4^3)$ -nets intersect the 4^4 -nets at approximately 60° , creating the appearance of triangular windows.

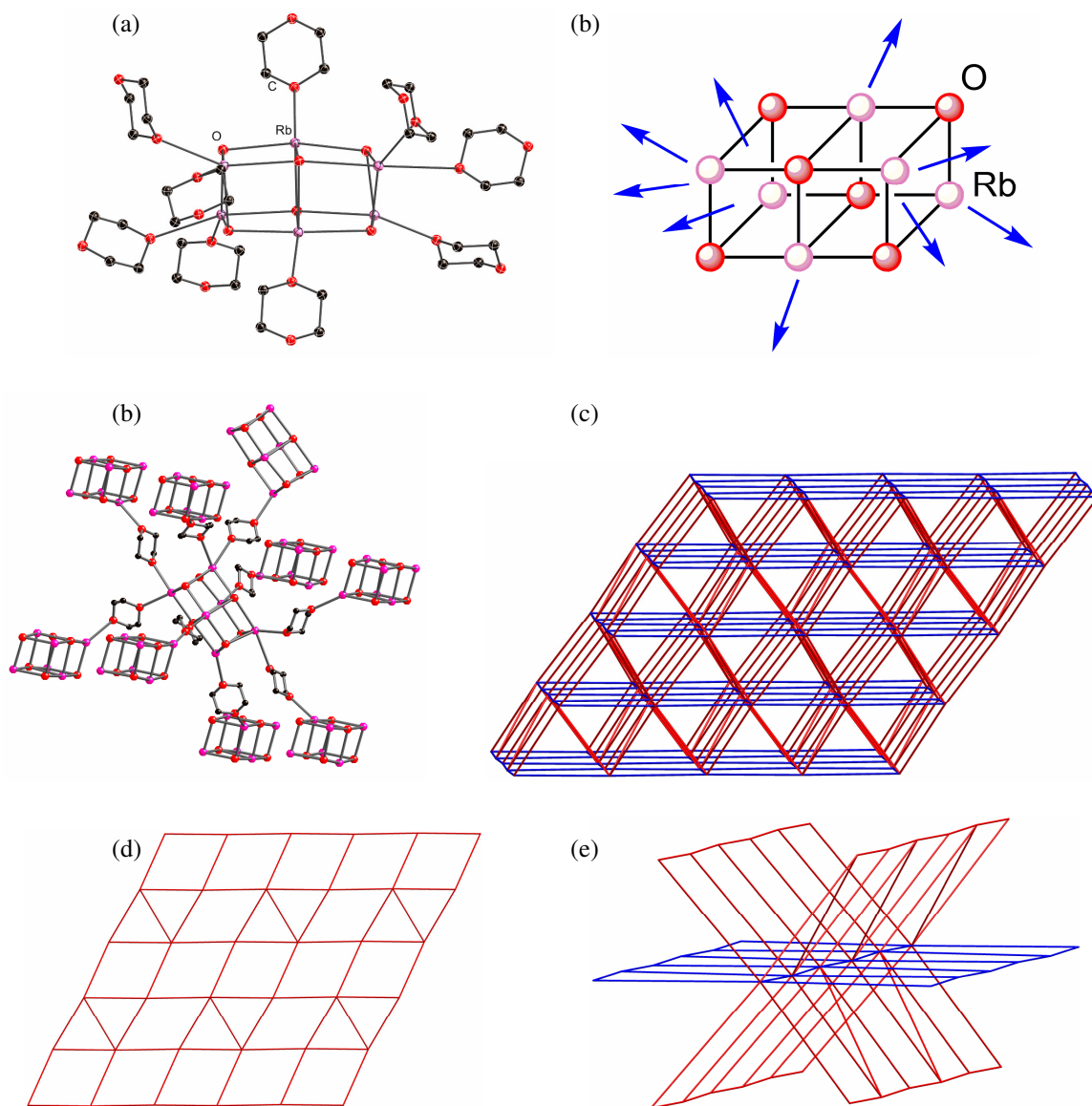


Figure 5.22 (a) Hexameric aggregate of $[2\text{-}i\text{Pr-C}_6\text{H}_4\text{ORb}]_6 \bullet (\text{diox})_{4.5}]_\infty$, **5.8** coordinated by nine dioxanes. The carbon atoms of the aryl ligand and hydrogen atoms are removed for clarity (b) Illustration of the nine points of network extension (c) Dioxane bridges to nine other aggregates. (d) The extended **ncd** network showing the framework with the 4^4 -nets in blue and the $(3.4^3)(3^2.4^3)$ -nets in red. (e) Section of the $(3.4^3)(3^2.4^3)$ -net. (f) Offset pattern of the two $(3.4^3)(3^2.4^3)$ -nets intersecting with a 4^4 -net.

5.4 Reactions of 2-Ethylphenol and 2-Methylphenol

5.4.1 Synthesis

To determine if water encapsulation is specific to the sterically demanding 2-*tert*-butylphenol and 2-isopropylphenol ligands or a more general phenomenon for this class of *ortho*-substituted compounds, the closely-related ligands 2-ethylphenol and 2-methylphenol were studied. Subsequently, the potassium complexes of both $[(2\text{-Et-C}_6\text{H}_4\text{OK})_{14}\cdot(2\text{-Et-C}_6\text{H}_4\text{OH})\cdot(\text{dioxane})_{12}]_{\infty}$ (**5.9**) and $[(2\text{-Me-C}_6\text{H}_4\text{OK})_4\cdot(\text{dioxane})_4]_{\infty}$ (**5.10**) were synthesized from dioxane. These two compounds are placed together because neither form a water encapsulated complex, but are still interesting because of their extended structure.

5.4.2 Structure of Potassium 2-Ethylphenoxide Dioxane

The dioxane solvate of potassium 2-ethylphenoxide, $[(2\text{-Et-C}_6\text{H}_4\text{OK})_{14}\cdot(2\text{-Et-C}_6\text{H}_4\text{OH})\cdot(\text{dioxane})_{12}]_{\infty}$ (**5.9**), has both a complicated local and extended structure. The localized structure is composed of a dimeric aggregate as well as two hexameric aggregates that have four and eight points of network extension, respectively (Figure 5.23).

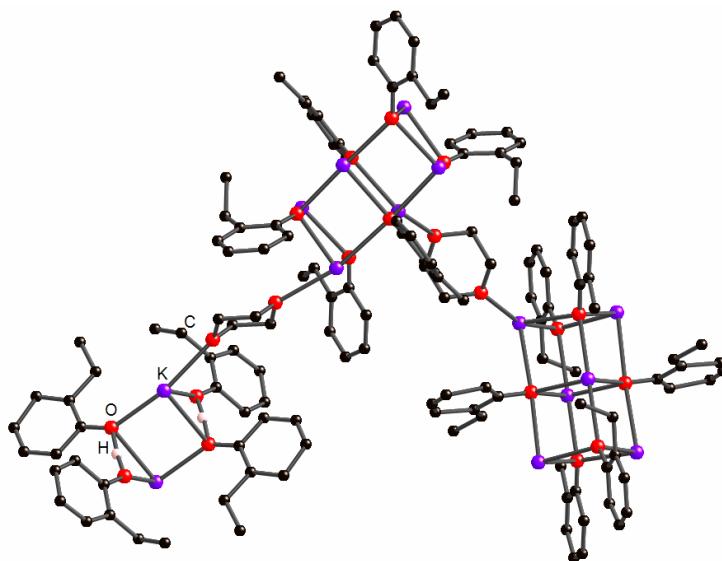


Figure 5.23 Structure of **5.10**, showing the two hexameric and one dimeric aggregate that make up the extended structure. The dioxane molecules and hydrogen atoms removed for clarity.

It should be noted that the X-ray structure could not be fully refined. The structure solved in two space groups, $C2/m$ ($R_1 = 7.92\%$) and $P2_1/c$ ($R_1 = 15.28\%$), although both solutions showed nearly full model disorder. Regardless, both solutions gave the same overall structure for both the localized and extended structure. The structure is only presented here to help continue to the study of *ortho*-substituted phenols and because of the completely novel topology it possesses.

The two hexameric aggregates are both coordinated by eight molecules of dioxane although the coordination is different in the two hexamers. The first hexamer has four potassiums each coordinated by one dioxane molecule and two potassiums that are coordinated by two dioxanes, whereas the second hexamer has two potassiums that are unsolvated and four potassiums that are coordinated by two dioxanes each. The dioxanes coordinated to both hexamers bridge to other aggregates. The reported bond distances

(Table 5.1) are not completely accurate because the refinement could not be completely finalized.

The dimeric aggregate is coordinated by a total of six dioxane molecules, although only four bridge to other aggregates. In addition the dimer is solvated by two molecules of non-deprotonated phenol.

Since there are eight bridging dioxane molecules associated with each of the hexameric aggregates and four bridging dioxane with the dimer, a rather complicated 3D structure is formed (Figure 5.24). The extended trinodal net is formally considered a (4,8)-connected net with stoichiometry $(4-C)(8-C)_3$, where C is the connectivity. This means that for every one 4-connected dimers there are three 8-connected hexamers. Although not shown here, the actual asymmetric unit consists of one full hexamer as well as one half hexamer and one half dimer. Symmetry operations on the asymmetric unit gives the $(4-C)(8-C)_3$ connectivity. The Schläfli symbol for this net is $(3^4.4^{10}.5^8.6^6)_2(3^4.4^{14}.5^6.6^4)(4^4.5^2)$ and the $td10=3014$. This topology does not yet have a code in the RCSR database. There are two recent reports of (4,8)-connected nets but neither can be considered a trinodal net like **5.10**.²⁴

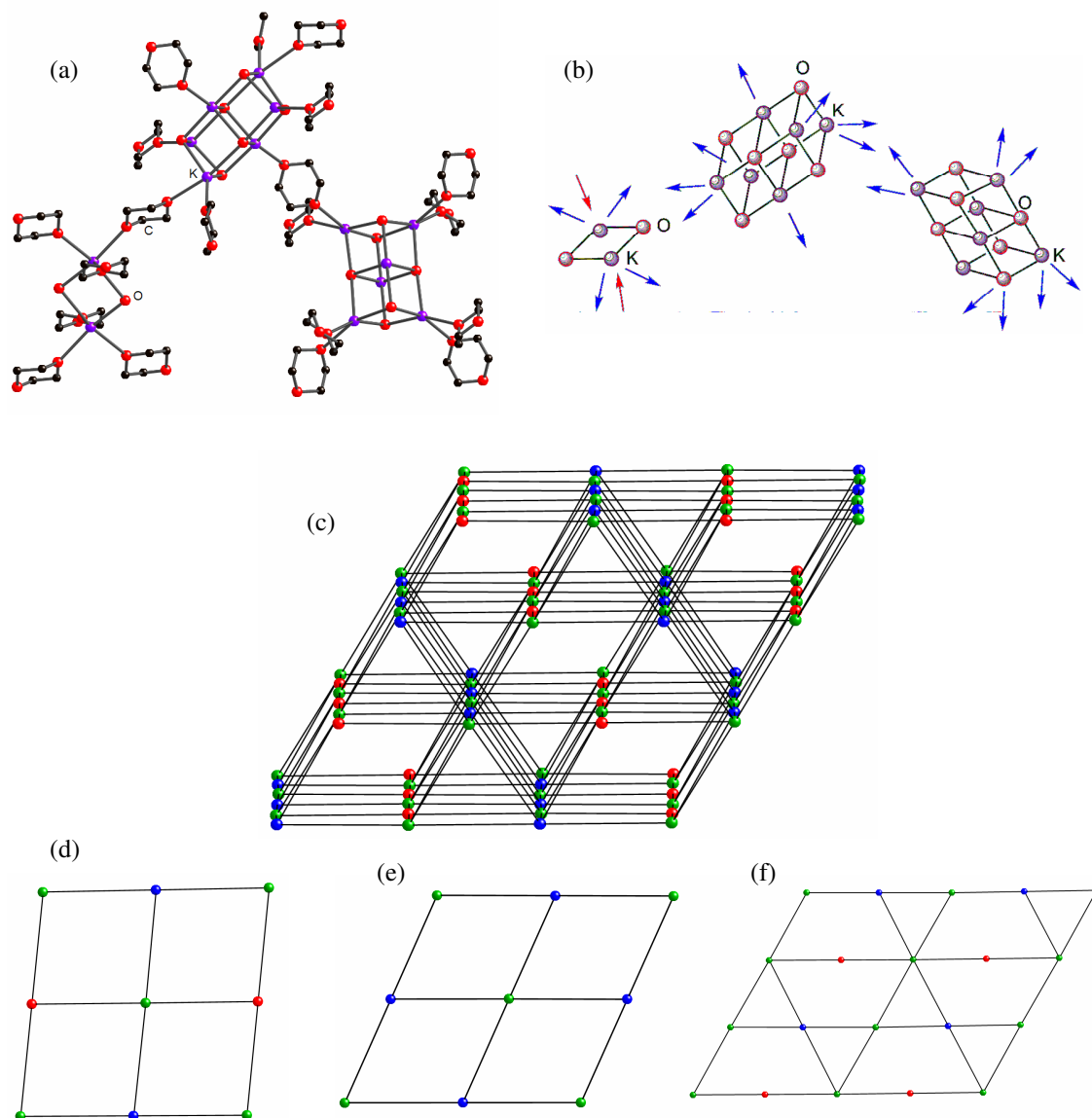


Figure 5.24 (a) The three aggregates of **5.10** coordinated by twenty dioxane molecules. The carbon atoms of the aryl ligand and hydrogen atoms are removed for clarity (b) Illustration of the points of network extension from each aggregate. (c) Extended network showing the dimeric (red) and hexameric (blue and green) aggregates as spheres. (d) Section of the three subnets with 4^4 , 4^4 , and $(3.5.3.5)_2(3.5^2.3.5^2)$ topology.

The complicated 3D net can be broken down into simpler subnets. There is a parallel series of 4^4 -nets that is composed of all three types of nodes (red, green, and blue spheres in Figure 5.24d). There is also a second series of 4^4 -nets that intersect the first

series at approximately 60°, which are composed of only the two 8-connected nodes (green and blue spheres). Finally there is a third, rather complicated subset that intersects both of the previous two subnets. The subnet has a Schläfli symbol of $(3.5.3.5)_2(3.5^2.3.5^2)$.

5.4.3 Structure of Potassium 2-Methylphenoxide Dioxane

The aggregate in the dioxane solvate of potassium 2-methylphenoxide, $[(2\text{-Me-C}_6\text{H}_4\text{OK})_4 \cdot (\text{dioxane})_4]_\infty$ (**5.10**), is unique for this series because it is the only tetramer (Figure 5.25). As the steric bulk at the *ortho*-position is decreased, it is unexpected that the aggregation state would also decrease. Moreover, the pyridine solvate of potassium 2-methylphenoxide is a hexamer.¹⁹ The aggregation state usually increases in a less polar solvents. The metrical parameters, as shown in Table 5.1, are in line though with the hexameric potassium structures reported in the previous sections.

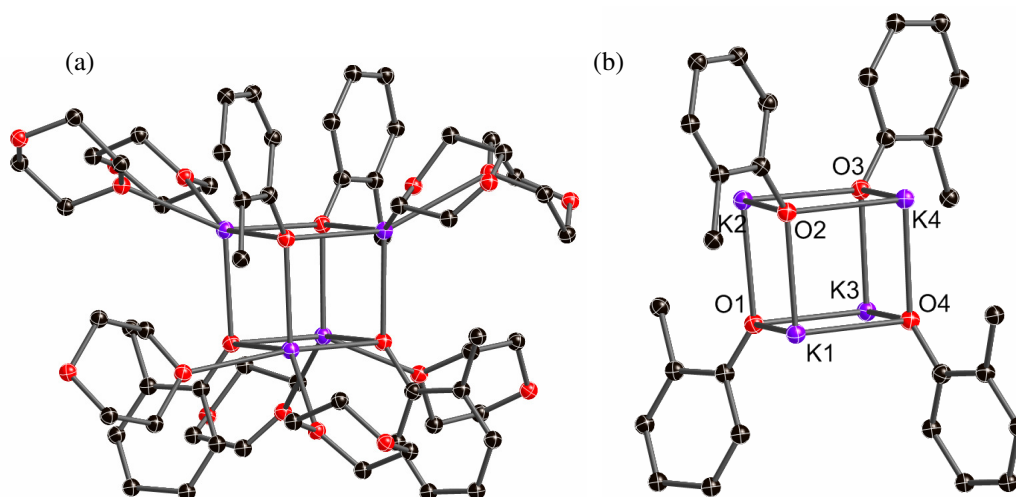


Figure 5.25 Structure of **5.10**, showing (a) the full tetrameric aggregate with eight coordinated dioxanes, and (b) a simplified view of the aggregate with dioxane molecules and hydrogen atoms removed for clarity.

The decreased aggregate size allows each of the four potassium centers to be coordinated by two dioxanes. All eight dioxanes bridge to other aggregates, however four of the dioxanes are involved in double bridges (Figure 5.26). The aggregate is therefore considered a 6-connected node. All of the 6-connected networks reported by our group thus far have always adopted the high-symmetry primitive cubic (**pcu**) topology. In fact, the **pcu** topology accounts for approximately 95% of all uninodal 6-connected frameworks.²⁵ Surprisingly, the extended structure of **5.8** does not adopt the **pcu** topology, but instead adopts a topology with a Schläfli symbol of $4^8.5^4.6^3$. This entirely novel topology is given the code **sxc** in the RCSR database.

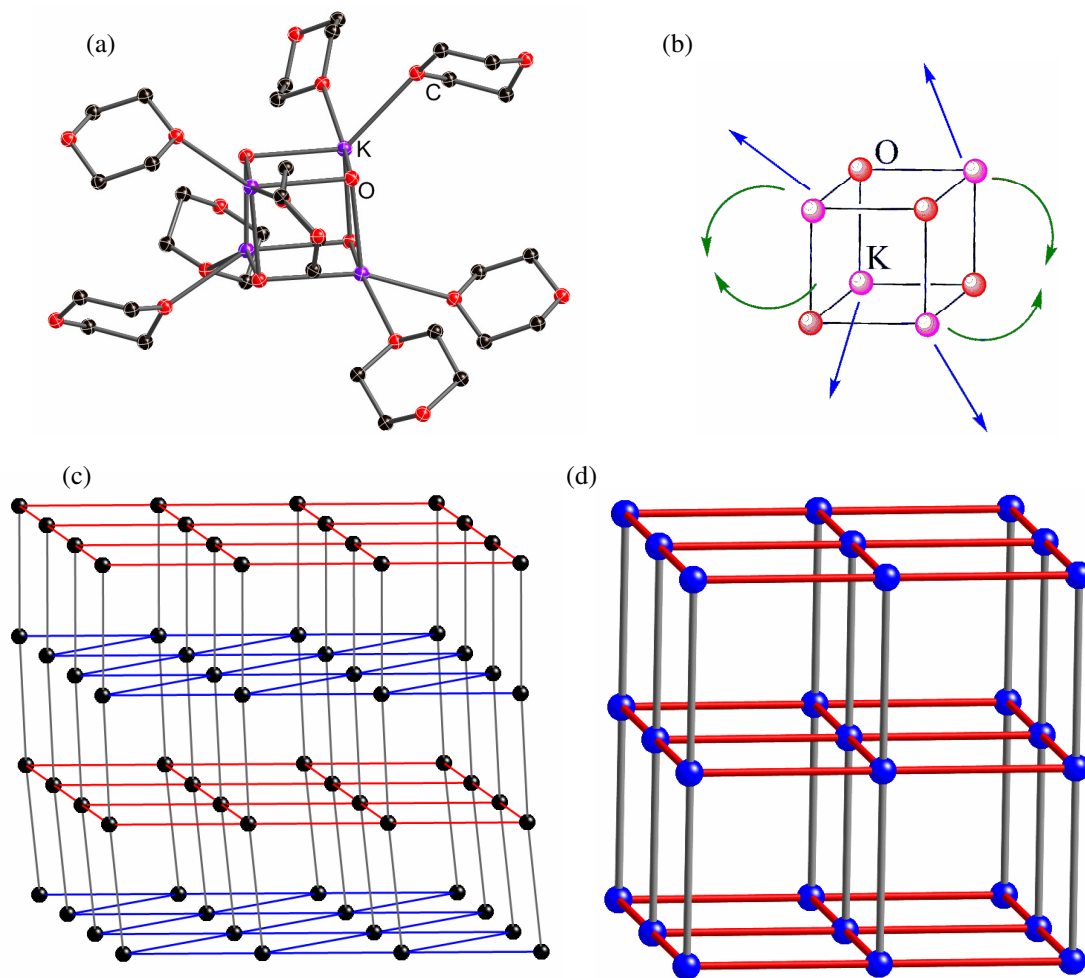


Figure 5.26 (a) Tetrameric aggregate of **5.10** coordinated by eight dioxanes. The carbon atoms of the aryl ligand and hydrogen atoms are removed for clarity. (b) Illustration of the eight bridging dioxanes. The four single dioxane bridges are shown in blue and the four dioxane double bridges are shown in green. (d) The 3D **sxc** net topology showing the framework with the 4⁴-nets in red and blue and the 6⁴-nets in gray. (e) The **pcu** net topology used for comparison.

In the **pcu** net, parallel sheets of 4⁴-nets are intersected along the ring edge by a perpendicular series of 4⁴-nets. In the **sxc** net, there are parallel sheets of 4⁴-nets but each sheet is slightly rotated with respect to the sheet above and below (shown as the red and blue sheets in Figure 5.22). This creates a vertical series of parallel nets (shown in gray) that have 6⁴ topology rather than 4⁴. Similar to the series of 7-connected topologies seen

in Chapter 4, these slight variations in connectivity give entirely new and unexpected topologies.

5.5 Summary

In conclusion, the characterization of *ortho*-substituted aryloxides, namely **5.1** – **5.7**, demonstrates that guest water molecules can be encapsulated within appropriately designed alkali metal host aggregates. Indeed, considering that the identification of water within **5.2** was overlooked in the literature, it is likely that similar neutral solvates have previously been prepared but not recognized. Future work in this area will most likely be directed towards determining the specificity of water encapsulation to a broader range of substituted aryloxides and also to other alkali metal aggregates.

This series of compounds is also notable for their ability to form high-connectivity nets as well as unique low-connectivity nets. Most notable is the formation of the first 9-connected network. Although exceedingly complex, the 9-connected structure of **5.8**, shows only the first of many beautiful topological possibilities for this degree of connectivity. Also of note is the novel trinodal (4,8)-connected net of **5.9** and the chiral 6-connected net of **5.10**. These early investigations into high-connectivity networks suggest that a fascinating and rich coordination chemistry is waiting to be discovered. Our hope is that underlying structural patterns will emerge from the systematic synthesis and classification of a library of high-connectivity networks, as has been evolved for their lower-connectivity counterparts.

5.6 Experimental Section

5.6.1 General Procedures

All experimental manipulations were performed under a dry nitrogen atmosphere using standard Schlenk techniques, or in an argon-filled glovebox.²⁶ All glassware was flame-dried under vacuum before use. Hexane was dried immediately before use by passage through columns of copper-based catalyst and alumina (Innovative Technology), and stored over 4 Å molecular sieves. Dioxane was purchased from Acros and was distilled over sodium benzophenone under N₂ prior to use. The phenols were purchased from Aldrich and were distilled over CaH₂ under N₂ prior to use. KHMDS was purchased from Aldrich and was used as received. Deuterated solvents were purchased from Cambridge Isotope Laboratories and were dried by storage over 4 Å molecular sieves. ¹H and ¹³C NMR spectra were recorded on either a Varian Unity Plus 300 MHz or a Bruker AVANCE DPX-400 spectrometer at 293 K, and were referenced internally to the residual signals of the deuterated solvents.

5.6.2 IR Spectroscopic Analysis

IR spectra were recorded on a Perkin-Elmer Paragon 1000 FTIR spectrometer. Samples were prepared as Nujol mulls using KBr plates.

5.6.3 Computational Details

The Gaussian 03 series of programs was used for the geometry optimization calculations.²⁷ No symmetry constraints were imposed and the molecules were allowed to

freely optimize at the HF/6-31G* level using related crystal structure data as starting geometries.

5.6.4 X-ray Crystallography

Crystals were examined under Infineum V8512 oil. The datum crystal was affixed to a thin glass fibre mounted atop a tapered copper mounting-pin and transferred to the 100 K nitrogen stream of a Bruker APEX II diffractometer equipped with an Oxford Cryosystems 700 series low-temperature apparatus. Cell parameters were determined using reflections harvested from three sets of 20 0.3° ω scans. The orientation matrix derived from this was passed to COSMO to determine the optimum data collection strategy.²⁸ Cell parameters were refined using reflections with $I \geq 10\sigma(I)$ harvested from the entire data collection. All data were corrected for Lorentz and polarization effects, as well as for absorption. Tables A.6, A.7, and A.8 list the key crystallographic parameters for **5.1-5.10**. The structures were solved and refined using SHELXTL.²⁹ Structure solution was by direct methods. Non-hydrogen atoms not present in the direct methods solution were located by successive cycles of full-matrix least-squares refinement on F^2 . All non-hydrogen atoms were refined with parameters for anisotropic thermal motion. Hydrogen atoms were placed at idealized geometries and allowed to ride on the position of the parent atom. Hydrogen thermal parameters were set to 1.2× the equivalent isotropic U of the parent atom, 1.5× for methyl hydrogens.

5.6.5 Neutron Data Collection

Neutron diffraction data were obtained at the Intense Pulsed Neutron Source (IPNS) at Argonne National Laboratory using the time-of-flight Laue single-crystal

diffractometer (SCD).^{30,31} At the IPNS, pulses of protons are accelerated into a heavy-element target 30 times a second to produce pulses of neutrons by the spallation process. Exploiting the pulsed nature of the source, neutron wavelengths are determined by time-of-flight based on the de Broglie equation $\lambda = (h/m) \cdot (t/l)$, where h is Planck's constant, m is the neutron mass, and t is the time-of-flight for a flight path l , so that the entire thermal spectrum of neutrons can be used. With two position-sensitive area detectors and a range of neutron wavelengths, a solid volume of reciprocal space is sampled with each stationary orientation of the sample and the detectors. The SCD has two ^6Li -glass scintillation position-sensitive area detectors, each with active areas of $15 \times 15 \text{ cm}^2$ and a spatial resolution of $< 1.5 \text{ mm}$. One of the detectors is centered at a scattering angle of 75° and a crystal-to-detector distance of 23 cm , and the second detector is at 120° and 18 cm . Details of the data collection and analysis procedures have been published previously.³²

A crystal of $\mathbf{1_n}$, with approximate dimensions of $2 \times 2 \times 1 \text{ mm}^3$, was wrapped in aluminum foil and glued to an aluminum pin that was mounted on the cold stage of a closed-cycle helium refrigerator. The crystal was then cooled to $100 \pm 1 \text{ K}$. For each setting of the diffractometer angles, data were stored in three-dimensional histogram form with coordinates x, y, t corresponding to horizontal and vertical detector positions and the time-of-flight, respectively. An auto-indexing algorithm³³ was used to obtain an initial orientation matrix from the peaks in three preliminary histograms measured for 60 minutes each. This unit cell approximately matched the previously reported X-ray unit cell indicating that the neutron sample was the correct material. For intensity data collection, runs of 7 hours per histogram were initiated for the data set. Settings were

arranged at χ and ϕ values suitable to cover at least one unique hemisphere of reciprocal space (Laue symmetry $2/m$). With the above counting times, 17 histograms were completed in the 6 days available for the experiment. Bragg peaks in the recorded histograms were indexed and integrated using individual orientation matrices for each histogram, to allow for any misalignment of the sample. Intensities were integrated about their predicted locations and were corrected for the Lorentz factor, the incident spectrum, and the detector efficiency. A wavelength-dependent spherical absorption correction was applied using cross sections from Sears³⁴ for the nonhydrogen atoms and from Howard *et al.*³⁵ for the hydrogen atoms ($\mu \text{ (cm}^{-1}\text{)} = 1.373 + 1.893 \lambda$). Symmetry related reflections were not averaged since different extinction factors are applicable to reflections measured at different wavelengths.

The GSAS software package was used for structural analysis.³⁶ The atomic positions of the X-ray diffraction structure were used as a starting point in the refinement. The refinement was based on F^2 reflections with a minimum d -spacing of 0.7 Å. Weights were assigned as $w(F_o^2) = 1 / [(\sigma(F_o^2) + (F_o^2))^2]$ where $\sigma^2(F_o^2)$ is the variance based on counting statistics and then multiplied by $\min(F_o/F_c, F_c/F_o)^4$. A joint refinement using X-ray and neutron reflections was used in the final model due to the large number of parameter variables (973 total variables). A total of 37,481 reflections were used in the refinement from the X-ray data and 7,651 reflections were used from the neutron data. However, only the neutron data was used to calculate the difference Fourier map. In the final refinement all heavy atoms, and all C-H hydrogen atoms were refined with anisotropic displacement parameters. Hydrogen atoms bound to the encapsulated water molecule were clearly located in the difference Fourier maps as determined by neutron

diffraction and were refined with isotropic displacement parameters. The site occupancy of the central water molecule was allowed to freely refine to 0.488(2). The hydrogens of the water molecule (H_a and H_b) were set to have the same site occupancy. After final refinement the maximum peak of unmodeled scattering density in the difference Fourier map was 0.711 fm \AA^{-3} . Data collection and refinement parameters are summarized in Table A.6.

5.6.6 Preparation and Characterization

5.1 and 5.1_n $[\{(2\text{-}t\text{Bu-C}_6\text{H}_4\text{OK})_6\supset(\text{H}_2\text{O})\}\cdot(\text{dioxane})_4]_\infty$ - KHMDS (3 mmol, 598 mg) was added to a stirred solution of 2-*t*-butylphenol (3 mmol, 0.4 mL) in dioxane (35 mL). A white precipitate formed, which completely dissolved on heating the solution to reflux. Water (6 mmol, 0.108 g) was then added to the solution at reflux. X-ray quality crystals were obtained by slowly cooling the resulting solution in a hot water bath. Crystalline yield: 480 mg, 64.0 %. δ_H (d_2 -CD₂Cl₂, 293K): 1.38 (s, 54H, C(CH₃)₃), 3.63 (s, 32H, Diox), 6.26 (d, $^3J_{H,H}=8$ Hz, 6H, *o*-H, Ar), 6.35(t, $^3J_{H,H}=8$ Hz, 6H, *m*-H, Ar), 6.89 (t, $^3J_{H,H}=8$ Hz, 6H, *p*-H, Ar), 7.14 (d, $^3J_{H,H}=8$ Hz, 6H, *m*-H, Ar).

5.2 $[\{(2\text{-}t\text{Bu-C}_6\text{H}_4\text{OK})_6\supset(\text{H}_2\text{O})\}\cdot(\text{THF})_6]$ - KHMDS (3 mmol, 598 mg) was added to a stirred solution of 2-*t*-butylphenol (3 mmol, 0.4 mL) in hexane (15 mL) and THF (3 mL). A white precipitate formed, which completely dissolved on heating the solution to reflux. X-ray quality crystals were obtained by slowly cooling the resulting solution in a hot water bath. Crystalline yield: 545 mg, 72.7 %. δ_H (d_8 -THF, 293K): 1.42 (s, 54H, C(CH₃)₃), 6.17 (d, $^3J_{H,H}=8$ Hz, 6H, *o*-H, Ar), 6.49(t, $^3J_{H,H}=8$ Hz, 6H, *m*-H, Ar), 6.72 (t, $^3J_{H,H}=8$ Hz, 6H, *p*-H, Ar), 6.95 (d, $^3J_{H,H}=8$ Hz, 6H, *m*-H, Ar).

5.3 $[\{(2\text{-}t\text{Bu-C}_6\text{H}_4\text{ORb})_6\supset(\text{H}_2\text{O})\}\cdot(\text{dioxane})_4\cdot(\text{dioxane})]_\infty$ - $[\text{RbOBu}^+\text{Bu}^+\text{OH}]_\infty$

(2 mmol 460 mg) was added to a stirred solution of 2-*t*-butylphenol (3 mmol, 0.31 mL) in hexane (9 mL) and dioxane (5 mL). A white precipitate formed, which completely dissolved on heating the solution to reflux. X-ray quality crystals were obtained by slowly cooling the resulting solution in a hot water bath. Crystalline yield: 230 mg, 30.5 %. δ_{H} (d_6 -DMSO, 293K): 1.09 (s, 54H, $\text{C}(\text{CH}_3)_3$), 3.56 (s, 32H, Diox), 5.58 (t, $^3J_{\text{H,H}}=8$ Hz, 6H, *m*-H, Ar), 5.71 (d, $^3J_{\text{H,H}}=8$ Hz, 6H, *o*-H, Ar), 6.33 (t, $^3J_{\text{H,H}}=8$ Hz, 6H, *p*-H, Ar), 6.57 (d, $^3J_{\text{H,H}}=8$ Hz, 6H, *m*-H, Ar).

5.4 $[\{(2\text{-}t\text{Bu-C}_6\text{H}_4\text{ONa})_6\supset(\text{H}_2\text{O})\}\cdot(\text{dioxane})_3]_\infty$ - NaH (3 mmol, 72 mg) was

added to a stirred solution of 2-*t*-butylphenol (3 mmol, 0.31 mL) in dioxane (25 mL). A white precipitate formed, which completely dissolved on heating the solution to reflux. X-ray quality crystals were obtained by slowly cooling the resulting solution in a hot water bath. Crystalline yield: 715 mg, 92.5 %. δ_{H} (d_6 -DMSO, 293K): 1.31 (s, 54H, $\text{C}(\text{CH}_3)_3$), 3.56 (s, 24H, Diox), 5.75 (t, $^3J_{\text{H,H}}=8$ Hz, 6H, *m*-H, Ar), 5.96 (d, $^3J_{\text{H,H}}=8$ Hz, 6H, *o*-H, Ar), 6.53 (t, $^3J_{\text{H,H}}=8$ Hz, 6H, *p*-H, Ar), 6.71 (d, $^3J_{\text{H,H}}=8$ Hz, 6H, *m*-H, Ar).

5.5 $[\{(2\text{-}i\text{Pr-C}_6\text{H}_4\text{OK})_6\supset(\text{H}_2\text{O})\}\cdot(\text{dioxane})_5\cdot(\text{dioxane})]_\infty$ - KHMDS (3 mmol,

598 mg) was added to a stirred solution of 2-*i*-propylphenol (3 mmol, 0.4 mL) in dioxane (4 mL) to give a white precipitate. The dioxane was removed completely *in vacuo* to give a white powder. Hexane (15 mL) and dioxane (5 mL) was added, which completely dissolved the precipitate on heating the solution to reflux. Water (0.7 mmol, 0.012 g) was then added to the solution while at reflux. X-ray quality crystals were obtained by slowly cooling the resulting solution in a hot water bath. Crystalline yield 320 mg, 40.2 %. δ_{H} ($\text{d}_2\text{-CD}_2\text{Cl}_2$, 293K): 1.18 (s, 36H, $\text{CH}(\text{CH}_3)_2$), 3.07 (multiplet, $^3J_{\text{H,H}} = 8.0$ Hz 6H,

$CH(CH_3)_2$), 3.63 (s, 48H, Diox), 6.24 (d, $^3J_{H,H} = 8.0$ Hz, 6H, *o*-H, Ar), 6.33 (t, $^3J_{H,H} = 8.0$ Hz, 6H, *m*-H, Ar), 6.88 (t, $^3J_{H,H} = 8.0$ Hz, 6H, *p*-H, Ar), 7.04 (d, $^3J_{H,H} = 8.0$ Hz, 6H, *m*-H, Ar). Note: although no water was seen in the 1H NMR, the doublet of the *ortho*-hydrogen is shifted downfield by 0.04 ppm compared to **5.6**.

5.6 [(2-*i*Pr-C₆H₄OK)₆·(dioxane)₅]_∞ - KHMDS (3 mmol, 598 mg) was added to a stirred solution of 2-*i*-propylphenol (3 mmol, 0.4 mL) in dioxane (4 mL) to give a white precipitate. All of the solvent was completely removed *in vacuo* leaving a dark yellow oil. The oil was taken up in hexane (5 mL), which gave a white precipitate after 5 minutes. Toluene (5 mL) and dioxane (5 mL) were added, which completely dissolved the precipitate on heating the solution to reflux. X-ray quality crystals were obtained by slowly cooling the resulting solution in a hot water bath. Yield: 680 mg, 91.5 %. δ_H (d₂-CD₂Cl₂, 293K): 1.19 (s, 36H, CH(CH₃)₂), 3.07 (multiplet, $^3J_{H,H} = 8.0$ Hz 6H, CH(CH₃)₂), 3.60 (s, 40H, Diox), 6.20 (d, $^3J_{H,H} = 8.0$ Hz, 6H, *o*-H, Ar), 6.33 (t, $^3J_{H,H} = 8.0$ Hz, 6H, *m*-H, Ar), 6.87 (t, $^3J_{H,H} = 8.0$ Hz, 6H, *p*-H, Ar), 7.04 (d, $^3J_{H,H} = 8.0$ Hz, 1H, *m*-H, Ar).

5.7 [{(2-^{*i*}Pr-C₆H₄OK)₆·(H₂O)₂·(dioxane)_{5.5}]_∞ - KHMDS (3 mmol, 598 mg) was added to a stirred solution of 2-*i*-propylphenol (3 mmol, 0.4 mL) in dioxane (4 mL) to give a white precipitate. The dioxane was removed completely *in vacuo* to give a white powder. Hexane (15 mL) was added which did not dissolve the precipitate. The solution was heated to reflux with dioxane (5 mL) and water (1.4 mmol, 0.024 g) added to solubilize the precipitate. X-ray quality crystals were obtained by slowly cooling the resulting solution in a hot water bath. Crystalline yield 370 mg, 47.4 % δ_H (d₂-CD₂Cl₂, 293K): 1.13 (s, 36H, CH(CH₃)₂), 3.06 (quintet, $^3J_{H,H} = 8.0$ Hz 6H, CH(CH₃)₂), 3.58 (s, 44H, Diox), 6.28 (d, $^3J_{H,H} = 8.0$ Hz, 6H, *o*-H, Ar), 6.33 (t, $^3J_{H,H} = 8.0$ Hz, 6H, *m*-H, Ar),

6.62 (s, 4H, H₂O), 6.86 (t, ³J_{H,H} = 8.0 Hz, 6H, *p*-H, Ar), 7.02 (d, ³J_{H,H} = 8.0 Hz, 6H, *m*-H, Ar)

5.8 [2-^{*i*}Pr-C₆H₄ORb)₆·(dioxane)_{4.5}]_∞ - [RbOBu^t·Bu^tOH]_∞ (2 mmol 460 mg) was added to stirred solution of 2-*i*-propylphenol (2 mmol, 0.27 mL) in dioxane (5 mL) to give a light yellow solution. All of the solvent was completely removed *in vacuo* to give a dark yellow oil. The oil was taken up in hexane (10 mL), which gave a white precipitate after 5 minutes. Complete dissolution was achieved by adding dioxane (5 mL) and heating the solution to reflux temperature. X-ray quality crystals were obtained by slowly cooling the resulting solution in a hot water bath. Crystalline yield: 225 mg, 39.2 %. δ_H (d₆-DMSO, 293K) 1.01 (s, 6H, CH₃, *i*Pr), 3.21 (multiplet, 1H, CH, *i*Pr), 3.56 (s, 6H, CH₂, dioxane), 5.73 (t, ³J_{H,H} = 8.0 Hz, 1H, *m*-H, Ar), 5.90 (d, ³J_{H,H} = 8.0 Hz, 1H, *o*-H, Ar), 6.49 (t, ³J_{H,H} = 8.0 Hz, 1H, *p*-H, Ar), 6.61 (d, ³J_{H,H} = 8.0 Hz, 1H, *m*-H, Ar).

5.9 [(2-Et-C₆H₄OK)₁₄·(2-Et-C₆H₄OH)·(dioxane)₁₂]_∞ - KHMDS (3 mmol, 598 mg) was added to a stirred solution of 2-ethylphenol (3 mmol, 0.35 mL) in hexane (10 mL) and dioxane (3 mL). A white precipitate formed, which completely dissolved on heating the solution to reflux. X-ray quality crystals were obtained by slowly cooling the resulting solution in a hot water bath. Crystalline yield: 154 mg, 26.8 %. δ_H (d₆-DMSO, 293K): 1.01 (t, ³J_{H,H}=8 Hz, 42H, CH₂CH₃), 2.36 (q, ³J_{H,H}=8 Hz, 28H, CH₂CH₃), 3.56 (s, 96H, Diox), 5.86 (t, ³J_{H,H}=8 Hz, 14H, *m*-H, Ar), 6.11 (d, ³J_{H,H}=8 Hz, 14H, *o*-H, Ar), 6.58 (t, ³J_{H,H}=8 Hz, 14H, *p*-H, Ar), 6.67 (d, ³J_{H,H}=8 Hz, 14H, *m*-H, Ar).

5.10 [(2-Me-C₆H₄OK)₄·(dioxane)₄]_∞ - KHMDS (3 mmol, 598 mg) was added to a stirred solution of 2-methylphenol (3 mmol, 0.35 mL) in hexane (5 mL) and dioxane (5 mL). A white precipitate formed, which completely dissolved on heating the solution to

reflux. X-ray quality crystals were obtained by slowly cooling the resulting solution in a hot water bath. Crystalline yield: 410 mg, 71.3 %. δ_{H} (d_6 -DMSO, 293K): 1.96 (s, 12H, CH_3), 3.56 (s, 32H, Diox), 5.85 (t, $^3J_{\text{H,H}}=8$ Hz, 14H, *m*-H, Ar), 6.12 (d, $^3J_{\text{H,H}}=8$ Hz, 14H, *o*-H, Ar), 6.55 (t, $^3J_{\text{H,H}}=8$ Hz, 14H, *p*-H, Ar), 6.68 (d, $^3J_{\text{H,H}}=8$ Hz, 14H, *m*-H, Ar).

5.7 References

- [1] (a) MacDougall, D. J.; Morris, J. J.; Noll, B. C.; Henderson, K. W. *Chem. Commun.* **2005**, 456. (b) MacDougall, D. J.; Noll, B. C.; Henderson, K. W. *Inorg. Chem.* **2005**, *44*, 1181. (c) Morris, J. J.; Noll, B. C.; Henderson, K. W. *Cryst. Growth Des.* **2006**, *6*, 1071. (d) Morris, J. J.; Noll, B. C.; Honeyman, G. G.; Kennedy, A. R.; Mulvey, R. E.; Henderson, K. W. *Chem. –Eur. J.* **2007**, *13*, 4418. (e) Morris, J. J.; Noll, B. C.; Henderson, K. W. *Chem. Commun.* **2007**, 5191. (f) Morris, J. J.; Noll, B. C.; Schultz, A. J.; Piccoli, P. M. B.; Henderson, K. W. *Inorg. Chem.* **2007**, *46*, 10473.
- [2] Wakefield, B. J. *Organolithium Methods*; Academic: London, 1988.
- [3] Wheatley, A. E. H. *Chem. Soc. Rev.* **2001**, *30*, 265.
- [4] McGarrity, J. F.; Ogle, C. A.; Brich, Z.; Loosli, H.-R. *J. Am. Chem. Soc.* **1985**, *107*, 1815.
- [5] *Molecular Clusters of the Main Group Elements*; Driess, M.; Nöth, H., Eds.; Wiley VCH: Weinham, 2004.
- [6] A water-solvated potassium aminosilanolate has previously been characterized: Reiche, C.; Kliem, S.; Klingebiel, U.; Noltemeyer, M.; Voit, C.; Herbst-Irmer, R.; Schmatz, S. *J. Organomet. Chem.* **2003**, *667*, 24.
- [7] Pluth, M. D.; Raymond, K. N. *Chem. Soc. Rev.* **2007**, *36*, 161.
- [8] Allen, F. H. *Acta Crystallogr.* **2002**, *B58*, 380.
- [9] Schultz, A. J.; Teller, R. G.; Williams, J. M.; Lukehart, C. M. *J. Am. Chem. Soc.* **1984**, *106*, 999.
- [10] Schultz, A. J.; De Lurgio, P. M.; Hammonds, J. P.; Mikkelsen, D.J.; Mikkelsen, R. L.; Miller, M. E.; Naday, I.; Peterson, P. F.; Porter, R. R.; Worlton, T. G. *Physica B* **2006**, 385-386, 1059.

- [11] Jeffery, G. A. *An Introduction to Hydrogen Bonding*; Oxford University Press: New York, NY, 1997.
- [12] (a) Barr, D.; Raithby, P. R.; Schleyer, P. v. R.; Snaith, R.; Wright, D. S. *J. Chem. Soc., Chem. Commun.* **1990**, 643. (b) Lambert, C.; Schleyer, P. v. R.; Pieper, U.; Stalke, D. *Angew. Chem. Int. Ed. Engl.* **1992**, 31, 77.
- [13] Jover, J.; Bosque, R.; Sales, J. *QSAR Comb. Sci.* **2007**, 26, 385.
- [14] Mikulcik, P.; Raithby, P. R.; Snaith, R.; Wright, D. S. *Angew. Chem. Int. Ed. Engl.* **1991**, 30, 428.
- [15] Boyle, T. J.; Andrews, N. L.; Rodriguez, M. A.; Campana, C.; Yiu, T. *Inorg. Chem.* **2003**, 42, 5357.
- [16] (a) Chisholm, M. H.; Drake, S. R.; Naiini, A. A.; Streib, W. E. *Polyhedron* **1991**, 10, 337. (b) Rabe, G. W.; Kheradmandan, S.; Liable-Sands, L. M.; Guzei, I. A.; Rheingold, A. L. *Angew. Chem., Int. Ed.* **1998**, 37, 1404. (c) Bilyk, A.; Hall, A. K.; Harrowfield, J. M.; Hosseini, M. W.; Skelton, B. W.; White, A. H. *Inorg. Chem.* **2001**, 40, 672.
- [17] Grob, T.; Harms, K.; Dehnicke, K. *Z. Anorg. Allg. Chem.* **2000**, 626, 1065.
- [18] (a) Long, D. -L.; Blake, A. J.; Champness, N. R.; Wilson, C.; Schröder, M. *Angew. Chem. Int. Ed.* **2001**, 40, 2443. (b) Luo, T. -T.; Tsai, H. -L.; Yang, S. -L.; Liu, Y. -H.; Yadav, R. D.; Su, C. -C.; Ueng, C. -H.; Lin, L. -G.; Lu, K. -L. *Angew. Chem. Int. Ed.* **2005**, 44, 6063. (c) Zhang, X. -M.; Fang R. -Q.; Wu, H. -S. *J. Am. Chem. Soc.* **2005**, 127, 7670. (d) Li, D.; Wu, T.; Zhou, X. -P.; Zhou, R.; Huang, X. -C. *Angew. Chem. Int. Ed.* **2005**, 44, 4175. (e) Fang, Q. -R.; Zhu, G. -S.; Jin, Z.; Xue, M.; Wei, X.; Wang, D. -J.; Qiu, S. -L. *Angew. Chem. Int. Ed.* **2006**, 45, 6126. (f) Zhang, J.; Kang, Y.; Zhang, J.; Li, Z. -J.; Qin, Y. -Y.; Yao, Y. -G. *Eur. J. Inorg. Chem.* **2006**, 2253.
- [19] Boyle, T. J.; Andrews, N. L.; Rodriguez, M. A.; Campana, C.; Yiu, T. *Inorg. Chem.* **2003**, 42, 5357.
- [20] Allen, F. H. *Acta Cryst.*, **2002**, B58, 380.
- [21] Rood, J. A.; Noll, B. C.; Henderson, K. W. *Inorg. Chem.* **2006**, 45, 5521.
- [22] Hill, R. J.; Long, D. L.; Champness, N. R.; Hubberstey, P.; Schroder, M. *Acc. Chem. Res.* **2001**, 34, 107.

- [23] (a) Shi, Y. -J.; Chen, X. -T.; Li, Y. -Z.; Xue, Z.; You, X. -Z. *New. J. Chem.* **2002**, 26, 1711. (b) Kang, Q. -Q.; Long, L. -S.; Huang, R. -B.; Zheng, L. -S. *Acta Crystallogr., Sect. E: Struct. Rep. Online* **2004**, E60, i12. (c) Jia, J.; Lin, X.; Wilson, C.; Blake, A. J.; Champness, N. R.; Hubberstey, P.; Walker, G.; Cussen, E. J.; Schröder, M. *Chem. Commun.* **2007**, 840. (d) Zhang, X.- M.; Zheng, Y. -Z.; Li, C. -R.; Zhang, W. -X.; Chen, X. -M. *Cryst. Growth Des.* **2007**, 7, 980.
- [24] (a) Borel, C.; Hakansson, M.; Ohrstrom, L. *CrystEngComm.* **2006**, 8, 666. (b) Zou, R.-Q.; Zhong, R.-Q.; Du, M.; Kiyobayashi, T.; Xu, Q. *Chem. Commun.* **2007**, 2467.
- [25] Ockwig, N. W.; Delgado-Friedrichs, O.; O'Keeffe, M.; Yaghi, O. M. *Acc. Chem. Res.* **2005**, 38, 176.
- [26] Schriver, D. F.; Drezdon, M. A. *The Manipulation of Air-Sensitive Compounds*, Wiley, New York, **1986**.
- [27] Gaussian 03, Revision C.01, Frisch, M. J.; Trucks, G. W.; Schlegel, H. B.; Scuseria, G. E.; Robb, M. A.; Cheeseman, J. R.; Montgomery, Jr., J. A.; Vreven, T.; Kudin, K. N.; Burant, J. C.; Millam, J. M.; Iyengar, S. S.; Tomasi, J.; Barone, V.; Mennucci, B.; Cossi, M.; Scalmani, G.; Rega, N.; Petersson, G. A.; Nakatsuji, H.; Hada, M.; Ehara, M.; Toyota, K.; Fukuda, R.; Hasegawa, J.; Ishida, M.; Nakajima, T.; Honda, Y.; Kitao, O.; Nakai, H.; Klene, M.; Li, X.; Knox, J. E.; Hratchian, H. P.; Cross, J. B.; Bakken, V.; Adamo, C.; Jaramillo, J.; Gomperts, R.; Stratmann, R. E.; Yazyev, O.; Austin, A. J.; Cammi, R.; Pomelli, C.; Ochterski, J. W.; Ayala, P. Y.; Morokuma, K.; Voth, G. A.; Salvador, P.; Dannenberg, J. J.; Zakrzewski, V. G.; Dapprich, S.; Daniels, A. D.; Strain, M. C.; Farkas, O.; Malick, D. K.; Rabuck, A. D.; Raghavachari, K.; Foresman, J. B.; Ortiz, J. V.; Cui, Q.; Baboul, A. G.; Clifford, S.; Cioslowski, J.; Stefanov, B. B.; Liu, G.; Liashenko, A.; Piskorz, P.; Komaromi, I.; Martin, R. L.; Fox, D. J.; Keith, T.; Al-Laham, M. A.; Peng, C. Y.; Nanayakkara, A.; Challacombe, M.; Gill, P. M. W.; Johnson, B.; Chen, W.; Wong, M. W.; Gonzalez, C.; Pople, J. A. Gaussian, Inc., Wallingford CT, **2004**.
- [28] J. Kaercher, *COSMO*, Bruker-Nonius AXS, Inc., Madison, Wisconsin, USA, **2003**.
- [29] G. M. Sheldrick, University of Göttingen, Göttingen (Germany), **2001**.
- [30] Schultz, A. J.; Teller, R. G.; Williams, J. M.; Lukehart, C. M., *J. Am. Chem. Soc.* **1984**, 106, 999.
- [31] Schultz, A. J., *Trans. Am. Crystallogr. Assoc.* **1987**, 23, 61.
- [32] Schultz, A. J.; Van Derveer, D. G.; Parker, D. W.; Baldwin, J. E., *Acta Cryst. C* **1990**, 46, 276.
- [33] Jacobson, R. A., *J. Appl. Cryst.* **1976**, 19, 283.

- [34] Sears, V. F., *In Methods of Experimental Physics, Vol. 23, Neutron Scattering, Part A.* ed.; Academic Press: Orlando, FL, 1986; 'Vol.' p 521.
- [35] Howard, J. A. K.; Johnson, O.; Schultz, A. J.; Stringer, A. M., *J. Appl. Cryst.* **1987**, *20*, 120.
- [36] Larson, A. C.; Von Dreele, R. B. *General Structure Analysis System--GSAS*, Los Alamos National Laboratory, **2000**.